The Importance of Mesozooplankton Diel Vertical Migration for Sustaining a Mesopelagic Food Web

Thomas B. Kelly[1,2,*], Peter C. Davison[3], Ralf Goericke[3], Michael R. Landry[3], Mark D. Ohman[3], Michael R. Stukel[1,2]

[1] Dept. of Earth, Ocean & Atmospheric Science, Florida State University, Tallahassee, FL, USA

[2] Center for Ocean-Atmospheric Prediction Studies, Florida State University, Tallahassee, FL, USA

[3] Integrative Oceanography Division, Scripps Institution of Oceanography, La Jolla, CA, USA

* Correspondence to Thomas B. Kelly (tbk14@fsu.edu)

Contribution to the Field

Understanding the flows of carbon within the ocean is important for predicting how global climate will shift; yet even after decades of research, the magnitude with which the ocean sequesters carbon is highly uncertain. One reason behind this uncertainty is that a variety of mechanisms control the balance between carbon input and carbon output within the ocean. The topic of this work is to inspect the role of biological organisms in physically transferring organic carbon from the surface to the deep ocean. As opposed to other mechanisms—such as sinking particles, the biological transfer of carbon is difficult to measure directly and is often quite variable, leading to large uncertainties. Here we use an extensive set of *in situ* observations off the coast of southern California to model the flow of carbon through the ecosystem. The model determined that in our study area nearly half of the total transfer of carbon from the surface ocean to deep was carried out by zooplankton that swim up to the surface each night to feed. This finding has direct implications for global carbon budgets, which often underestimate this transfer of carbon.

Keywords: Biological Carbon Pump, Export Production, DVM, LIEM, Inverse Model, Carbon Export, Ecosystem Model

Abstract

We used extensive ecological and biogeochemical measurements obtained from quasi-Lagrangian experiments during two California Current Ecosystem Long-Term Ecosystem Research cruises to analyze carbon fluxes between the epipelagic and mesopelagic zones using a linear inverse ecosystem model (LIEM). Measurement constraints on the model include ^{14}C primary productivity, dilution-based microzooplankton grazing rates, gut pigment-based mesozooplankton grazing rates (on multiple zooplankton size classes), ^{234}Th:^{238}U disequilibrium and sediment trap measured carbon export, and metabolic requirements of micronekton, zooplankton, and bacteria. A likelihood approach (Markov Chain Monte Carlo) was used to estimate the resulting flow uncertainties from a sample of potential flux networks. Results highlight the importance of mesozooplankton active transport (i.e., diel vertical migration) for supplying the carbon demand of mesopelagic organisms and sequestering carbon dioxide from the atmosphere. In nine water parcels ranging from a coastal bloom to offshore oligotrophic conditions, mesozooplankton active transport accounted for 18% - 84% (median: 42%) of the total carbon supply to the mesopelagic, with gravitational settling of POC (12% - 55%; median: 37%) and subduction (2% - 32%; median: 14%) providing the majority of the remainder. Vertically migrating zooplankton contributed to downward carbon flux through respiration and excretion at depth and via consumption loses to predatory zooplankton and mesopelagic fish (e.g. myctophids and gonostomatids). Sensitivity analyses showed that the results of the LIEM were robust to changes in nekton metabolic demands, rates of bacterial production, and mesozooplankton gross growth efficiency. This analysis suggests that prior estimates of zooplankton active transport based on conservative estimates of standard (rather than active) metabolism should be revisited.

2

1. Introduction

56
57   Although mesopelagic food webs are believed to depend entirely on productivity
58 generated in the euphotic zone, reconciling mesopelagic metabolic demand with estimates of
59 export has been challenging (Burd et al., 2010; del Giorgio and Duarte, 2002; Hannides et al.,
60 2015; Henson et al., 2011; Steinberg et al., 2008). Due to large uncertainties in rate
61 measurements for meso- and bathypelagic organisms as well as low sampling resolution, steady-
62 state budgets must either report wide ranges or otherwise exclude some processes, such as
63 mortality and defecation of diel vertical migrators at depth. Even among recent studies, global
64 carbon export budgets have been highly variable (Boyd and Trull, 2007; Henson et al., 2011,
65 2015; Laws et al., 2011; Siegel et al., 2014). Compounding this issue, several analyses have
66 reported carbon demands by mesopelagic bacteria alone that exceed calculated carbon export
67 (Burd et al., 2010; Ducklow and Harris, 1993), sometimes by an order of magnitude (Steinberg
68 et al., 2008). This apparent imbalance between the carbon supply to the mesopelagic and the
69 estimated metabolic demand suggests either export estimates fail to capture important dynamics
70 or that metabolic calculations are grossly overestimated (Burd et al., 2010). Notably, the most
71 prominent study to date that has purported to show a balanced epipelagic-mesopelagic carbon
72 budget did so by assuming much lower bacterial carbon:leucine ratios than used in other
73 estimates of bacterial production (Giering et al., 2014). Hence, their results may have been
74 derived from misinterpretation of bacterial leucine uptake.

75   Recent work has demonstrated that diel vertical migrators are important for net transfer of
76 organic carbon from the euphotic zone to the mesopelagic, a transfer not measured with
77 traditional carbon export methods (Morales, 1999; Steinberg et al., 2000). Since export by
78 mesozooplankton is not captured by sediment traps or chemical disequilibria, we must rely on
79 logistically difficult biomass-based estimates or on indirect modeling syntheses. For example,
80 using remote sensing fields and a size-structured ecosystem model, Archibald et al. (2019) found
81 that global zooplankton diel vertical migration (DVM) can increase export production by 14%
82 annually. This is consistent with previous modeling exercises based on zooplankton behavior
83 (Bianchi et al., 2013) and community size structure (Aumont et al., 2018). Zooplankton behavior
84 models argue that for DVM to be evolutionarily advantageous (Cohen and Forward, 2009), the
85 energy expenditure should be offset by a commensurate reduction in predation risk. Using this
86 modeled-behavior approach, Hansen and Visser (2016) found that 16% - 30% mid-latitude
87 export production in the North Atlantic was due to DVM mesozooplankton. Each of these
88 models note sensitivities to zooplankton biomass and the fraction of the zooplankton population
89 that undergoes DVM, which are ecosystem metrics that are difficult to generalize.

90   Linear inverse ecosystem models (LIEM) have been shown to be a versatile and robust
91 framework for integrating a wide range of ecosystem data (Gontikaki et al., 2011; Sailley et al.,
92 2013; Stukel et al., 2018b; van Oevelen et al., 2012; Vézina et al., 1988). An LIEM combines an
93 ecosystem network with observations and generalized constraints to determine possible energy
94 flows through the ecosystem. Unlike a forward model (e.g., an NPZ model; Franks, 2002), the

95 relationships between organisms are not prescribed by functional responses of model state
96 variables (e.g., assuming a Monod functional form controls phytoplankton nutrient uptake
97 responses or an Ivlev grazing formulation). Instead, the model includes all possible combinations
98 of fluxes that are compatible with the input constraints, and the most likely ecosystem structure
99 is then retrieved based on a random walk through the solution space (van den Meersche et al.,
100 2009). This inverted approach has the advantage of not requiring *a priori* assumptions of
101 ecological relationships but instead relies on many independent constraints on the food web.

102 The California Current Ecosystem (CCE) is an eastern boundary current upwelling biome
103 with extensive temporal and spatial variability. As a result of high mesozooplankton biomass and
104 strong DVM (Ohman and Romagnan, 2016; Powell and Ohman, 2015; Stukel et al., 2013), we
105 expect a substantial contribution to export production by diel vertical migrators and a
106 commensurately important role in satisfying the carbon demand of the mesopelagic. Stukel et al.
107 (2013) suggested that active transport could be responsible for 1.8 – 29% of total export in the
108 CCE. However, their study focused only on active transport fluxes due to zooplankton
109 respiration and used conservative assumptions. To more thoroughly investigate the potential
110 importance of active transport, we designed a two-layer LIEM, which includes non-living
111 organic matter, primary producers, zooplankton and planktivorous nekton organized into two
112 layers: an epipelagic and a mesopelagic ecosystem. Using extensive data from two cruises of the
113 CCE Long-Term Ecological Research (LTER) Program in the southern California Current region,
114 our LIEM data synthesis suggests that active transport of carbon from the epipelagic down to
115 depth is a significant mechanism supporting the mesopelagic carbon demand. Although previous
116 studies have indicated that active transport may be responsible for 10% - 30% of total carbon
117 flux (Archibald et al., 2019; Aumont et al., 2018; Bianchi et al., 2013; Hansen and Visser, 2016;
118 Yebra et al., 2005), our LIEM suggests that 20% - 80% of carbon export in the CCE may be the
119 result of DVM by mesozooplankton.

120

2. Materials and methods

121

2.1. Ecosystem data

122

123 The data presented here (Appendix A) were collected during two cruises of the California
124 Current Ecosystem Long Term Ecological Research (CCE LTER) program (P0704 in April 2007;
125 P0810 in Oct. 2008). On these cruises, *in situ* drift arrays were used for quasi-Lagrangian
126 tracking of water parcels for periods of 3-5 days (Landry et al., 2009, 2012), while the water
127 column was repeatedly sampled for the following variables: CTD-derived physical data,
128 phytoplankton diversity and biomass (flow cytometry, epifluorescence microscopy, and pigment
129 analyses, (Taylor et al., 2012)), primary production ($H^{14}CO_3$-uptake, (Morrow et al., 2018)),
130 mesozooplankton biomass and community analyses (paired day-night bongo and Multiple
131 Opening and Closing Net with Environmental Sampling System, MOCNESS net tows, (Ohman
132 et al., 2012; Powell and Ohman, 2012), microzooplankton biomass (epifluorescence microscopy),

133 microzooplankton grazing (dilution method, Landry et al., 2009), mesozooplankton grazing (gut
134 pigment methods, Landry et al., 2009), meso- and epipelagic micronekton biomass and
135 metabolic demands (see Section 2.1.1; Oozeki net trawls, multi-frequency EK60 echosounder,
136 and individual-based metabolic model (Davison et al., 2013, 2015), bacterial production (^{3}H-
137 leucine uptake, Samo et al., 2012), and gravitational particle export (sediment traps and
138 ^{234}Th:^{238}U disequilibrium, Stukel et al., 2013). The use of a quasi-Lagrangian sampling
139 framework also allowed us to assess net rates of change of phytoplankton biomass. Bulk rates
140 and associated errors for the 3-5 day cycles were calculated by averaging vertically-integrated
141 rates or biomasses for each experimental cycle. The data and detailed methods can be found on
142 the CCE LTER Datazoo website (http://oceaninformatics.ucsd.edu/datazoo/data/ccelter/datasets)
143 and/or in published manuscripts cited above.

144   The quasi-Lagrangian experiments (hereafter 'cycles') spanned much of the physical,
145 chemical, and ecological variability of the CCE domain (Table 1, Fig. 1) which allowed us to
146 classify cycles according to nutrient conditions, the primary driver of ecosystem variability
147 within the CCE (Landry et al., 2012). Cycle classification was defined as: nutrient-limited cycles
148 which were conducted in off-shore, low nutrient regions (P0704-2, P0810-2, P0810-6); transition
149 region cycles which were characterized by low surface nutrient concentrations and intermediate
150 NPP and biomass (P0810-1, P0810-3, P0810-4); and upwelling cycles in which surface nutrient
151 concentrations and phytoplankton growth rates were highest (P0704-1, P0704-4, P0810-5; Table
152 1).

2.1.1. Phytoplankton, Bacteria, and Protist Constraints

154   Daily *in situ* primary productivity measurements using $H^{14}CO_3^-$ uptake (^{14}CPP) were
155 conducted at 6-8 depths spanning the euphotic zone using 4 L incubations subsampled in
156 triplicate (Morrow et al., 2018). A 250 mL dark bottle was used to correct for non-photosynthetic
157 ^{14}C uptake. Contemporaneously, *in situ* dilution experiments, using the two-treatment approach
158 of Landry et al. (2008), were conducted to measure protistan zooplankton grazing rates (Landry
159 et al., 2009). Euphotic zone primary production and protistan zooplankton gazing rates were
160 vertically integrated and averaged by cycle.

161   Rates of ^{3}H-leucine incorporation into bacteria were measured in triplicate at multiple
162 depths during each cycle (Samo et al., 2012). Each profile was vertically integrated and then
163 averaged by cycle in order to determine epipelagic bacterial production rates. Additionally, an
164 upper and lower bound for mesopelagic bacterial production was calculated by integrating a
165 bacterial production attenuation curve and then scaling by the epipelagic bacterial production (Eq.
166 1).

167 $$Mesopelagic\ BP = BP_{100} \int_{100}^{450} \left(\frac{z}{z_0}\right)^{-\alpha} dz \qquad (1)$$

168 where BP_{100} is the measured BP rate at 100 m and α (BP attenuation factor) = 1.47 (Yokokawa et
169 al., 2013) for the lower limit and $\alpha = 0$ (i.e., no attenuation) for the upper limit.

5

2.1.2. Mesozooplankton and Nekton Constraints

Data for the mesozooplankton constraints primarily comes from either day-night paired oblique bongo net tows through the epipelagic (for grazing rates) or day-night paired MOCNESS tows taken at 9 depth horizons spanning the upper 450 m (for biomass and metabolism estimates). MOCNESS samples were analyzed by ZooScan digital scanner (Gorsky et al., 2010; Ohman et al., 2012), vignettes provisionally classified using machine learning methods, then 100% manually validated. Organisms were sorted (Stukel et al., 2013) into groups including euphausiids, nauplii, copepods, appendicularians, siphonophores, and other crustaceans. For this study, we separated the mesozooplankton community into two size classes (<1 mm and >1 mm) of grazers and one compartment for gelatinous predators (siphonophores). We also partitioned the large and small mesozooplankton into non-vertically migrating epipelagic residents, vertical-migrators, or mesopelagic resident communities. Biomass of the non-vertically migrating, epipelagic mesozooplankton was calculated from the upper 100 m net during daytime tows while the non-vertically migrating, mesopelagic biomass was calculated based on the nighttime mesopelagic (100 m – 450 m) net tows (Stukel et al., 2013). We note that epipelagic biomass estimates are likely conservative due to net avoidance. Biomass estimates for the DVM mesozooplankton were calculated by averaging the difference in the night and day epipelagic biomass estimates with the difference in the day and night mesopelagic biomass estimates. This approach was used in order to be the most consistent with both the epipelagic and mesopelagic biomass estimates for non-vertically migrating biomass. For a list of abbreviations used for all model compartments, see Table 2.

Minimum respiration for each mesozooplankton group was calculated using published temperature-length-basal respiration relationships (Ikeda et al., 2001). Oxygen consumption was converted to carbon units using the scale factor 9.88×10^{-3} mg C d^{-1} (μL O$_2$ hr^{-1})$^{-1}$. Mesozooplankton grazing on phytoplankton was calculated from gut pigment contents of oblique bongo net tow tows (202 μm mesh, D = 0.71m) and estimated gut passage rates (Dam and Peterson, 1988). Carbon-based grazing rates were then calculated from chlorophyll (Chl) consumption, and C:Chl ratios computed as the ratio of NPP to chlorophyll-specific growth rates obtained from the dilution experiments. Mesozooplankton grazing rates were size fractionated as above. Mesozooplankton gut contents samples were improperly frozen for P0810-5, P0810-6, and most of P0810-4. In order to provide estimates for these grazing rates, average grazing rates from the cycle with the same classification were used (e.g. P0810-5 was an upwelling cycle so grazing rates were averaged from the other upwelling cycles). Conservative uncertainty estimates were set to be 2x the error calculated by propagation of error. This higher level of uncertainty is a reasonable compromise given the data limitations. For additional details on gut pigment processing, see Landry et al. (2009).

Nekton biomass was estimated based on catches made by a 5 m^2 Matsuda-Oozeki-Hu net trawl (Davison et al., 2013). For each station, epipelagic net tows were conducted at night after the ascent of the deep scattering layer. Preserved specimens from each net tow were identified to species and measured. Fish were classified as either non-vertical migrating or vertically migrating based on species. An individual based model was then used to determine metabolic

6

211   rates and requirements for each nekton population: resident epipelagic, diel vertical migrant, and
212   resident mesopelagic (Davison et al., 2013).

213   **2.1.2. Export Production**

214   VERTEX-style sediment traps consisting of 8-12 tubes per depth were deployed and
215   recovered at the start and end of each cycle (Knauer et al., 1979; Stukel et al., 2013). Tubes were
216   filled with a hypersaline, poisoned brine solution. Upon recovery >200-µm swimming
217   mesozooplankton taxa were manually removed during inspection under a stereomicroscope.
218   Samples for C and N or C:^{234}Th ratios were filtered through pre-combusted glass fiber and quartz
219   filters, respectively, prior to analysis on a CHN elemental analyzer or a RISO beta multi-counter.

220   ^{234}Th:^{238}U disequilibrium measurements were made at 12 depths spanning the upper 200
221   m at the start and end of each cycle using standard small-volume procedures (Benitez-Nelson et
222   al., 2001; Pike et al., 2005). Thorium-234 export rates were then computed using a 1-box steady
223   state model (Savoye et al., 2006). The C:^{234}Th ratio measured from sediment trap particles was
224   used to convert to carbon export. For additional details, see (Stukel et al., 2019).

225   Subduction of POC provides an alternative mechanism for the export of organic matter to
226   the mesopelagic, that is not measured by either sediment traps or ^{234}Th profiles, which only
227   record gravitational settling of particles. A three-dimensional particle advection model was used
228   to determine a range of possible subduction rates (Stukel et al., 2018c). The maximum and
229   minimum estimates of particle subduction were used as bounds on two size-fractionated
230   subduction flows within the LIEM.

231

Table 1. Overview of conditions for each cycle along with the attributed classifications:
upwelling, transition region, and nutrient limited.

Cycle	Classification	Surface Chl (µg Chl a L^{-1})	^{14}C Primary Productivity (mg C m^{-2} d^{-1})	Mesozooplankton Biomass (mg C m^{-2})
P0704-1	Upwelling	1.35	1,233	2,695
P0704-2	Nutrient Limited	0.22	587	391
P0704-4	Upwelling	0.99	2,314	1,715
P0810-1	Transition region	0.45	554	740
P0810-2	Nutrient Limited	0.20	484	528
P0810-3	Transition region	0.72	892	923
P0810-4	Transition region	1.05	674	832

| P0810-5 | *Upwelling* | 1.47 | 1,672 | 1,098 |
| P0810-6 | *Nutrient Limited* | 0.22 | 325 | 628 |

232

2.2. Linear inverse model

233

234   We developed a LIEM for the CCE to investigate mechanisms of epipelagic-mesopelagic
235   coupling. The LIEM consists of 140 flows (i.e., ecosystem fluxes, Supp. Table 2) and 24
236   compartments (i.e. standing stocks; Table 2) organized into two layers: the surface epipelagic
237   and a deeper mesopelagic ecosystem (defined as 100 – 450 m depth to match with *in situ*
238   measurements). The epipelagic and mesopelagic ecosystems consist of 73 flows and 64 flows,
239   respectively, with four explicit flows (particle sinking and subduction) and three implicit flows
240   (active transport) directly linking the two layers (Figure 1). Three vertically migrating
241   compartments (small and large mesozooplankton and nekton) connect the epipelagic and
242   mesopelagic through a transfer associated with DVM (i.e. respiration, excretion, and mortality).
243   Constraints consist of 24 mass balance equations, 18 approximate equations (i.e. *in situ* rate
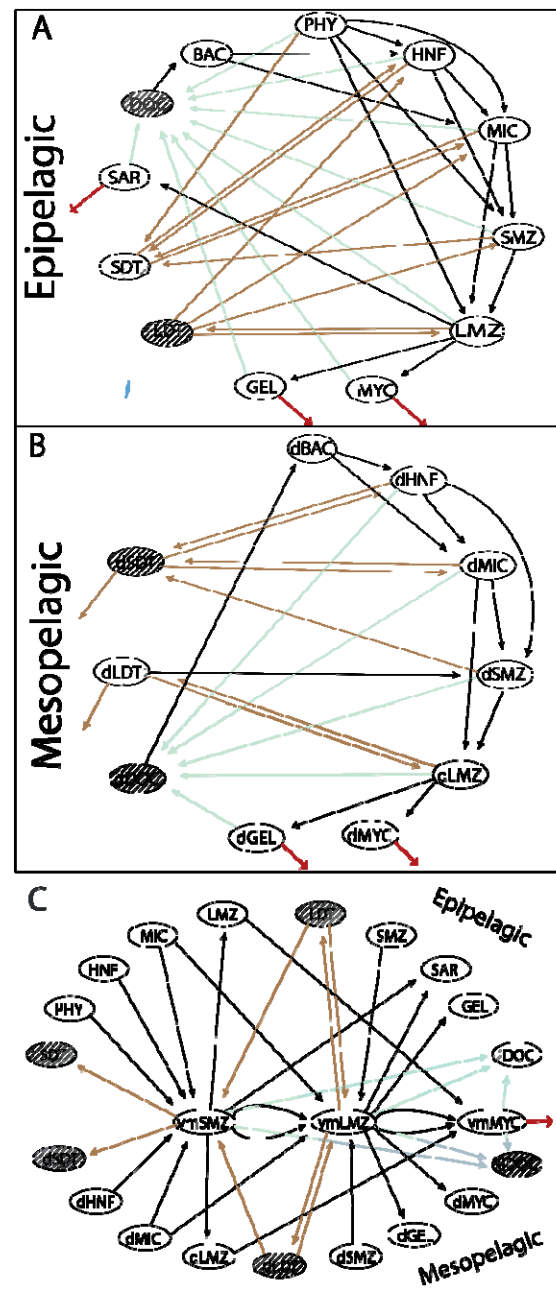244   measurements) and 133 inequalities, which are provided in the Online Supplement.

8

Figure 1. Schematic of model structure organized into distinct layers where arrows indicate a model flow. (A) Epipelagic organisms and POC. Arrows are colored for convenience: direct flows to the mesopelagic = blue, flows to HTL = red, flows to and from detritus = brown, and flows to DOC or dDOC = green. Shaded compartments indicate no losses to respiration. (B) Same as (A) for the mesopelagic. (C) Showing the connectivity between the epipelagic and mesopelagic layers via vertical migrators. See Table 2 for abbreviations.

The 18 approximate equations are ecosystem observations, which can be directly compared to flows within the model (Appendix A). These equations are net primary productivity

249 (NPP), phytoplankton biomass net rate of change, protistan grazing, size-fractionated grazing
250 rates (<1-mm and >1-mm) for epipelagic resident and DVM mesozooplankton, sediment trap
251 and ^{234}Th-based export fluxes, bacterial production, and mesopelagic fish respiration, mortality
252 and fecal pellet production rates. The model was provided an estimated value and associated
253 uncertainty for each measurement.

254 Respiration, mesopelagic export, nekton fecal pellets, and losses to higher trophic levels
255 were included as closure terms. Within the model every organism loses carbon to respiration,
256 DOC excretion, and defecation or mortality to detritus/fecal pellets. Grazing was allowed
257 between organisms whose ecological role and size-range permit grazing (e.g. small
258 mesozooplankton graze on nano- and microplankton; sardines consume only >1-mm
259 mesozooplankton). Mass balance was required for each compartment. All compartments were
260 assumed to be at steady state except for PHY, for which changes in biomass were measured (via
261 Chl-*a* proxy) during each cycle and incorporated into the model. This flexibility was essential to
262 capture the bloom-phase of the ecosystem since dramatic shifts in Chl-*a* were observed during
263 some cycles.

264

Table 2. Names and abbreviations of all model compartments. An abbreviation in the left column indicates inclusion in the epipelagic, while an abbreviation in the right column indicates inclusion in the mesopelagic. Each abbreviation is a distinct compartment in the LIEM with the prefix 'vm' signifying vertical migration and 'd' signifying the mesopelagic.

	Epipelagic Abbreviation	Name	Mesopelagic Abbreviation
Organisms	PHY	Phytoplankton	
	HNF	Heterotrophic Nanoflagellates	dHNF
	MIC	Microzooplankton	dMIC
	SMZ, vmSMZ	Small Mesozooplankton	dSMZ, vmSMZ
	LMZ, vmLMZ	Large Mesozooplankton	dLMZ, vmLMZ
	SAR	Sardines and other planktivorous fish	
		Non-DVM Myctophids	dMYC
	GEL	Gelatinous Predators	dGEL
	vmMYC	Vertically Migrating Myctophids	vmMYC
	BAC	Bacteria	dBAC
POC & DOC	SDT	Small Detritus	dSDT
	LDT	Large Detritus	dLDT
	DOC	Dissolved Organic Matter	dDOC
Closures	HTL	Higher Trophic Levels	HTL
	RES	Respiration	dRES
	FP	Fecal Matter	FP
		External	EXT

265

10

266

2.2.1. Inequality constraints

The formulas used in the inequality constraints are provided in the Online Supplement. Upper and lower limit estimates of POC subduction from the epipelagic to the mesopelagic layer were taken from (Stukel et al., 2018c), and a minimum fecal pellet flux was assigned based on the assumption that recognizable fecal pellets in sediment trap material represented a lower limit on total fecal pellet flux. Minimum and maximum Gross Growth Efficiencies (GGE) and Absorption Efficiencies (AE) were assigned according to previously accepted literature values: 10% – 40% GGE for protistan zooplankton (HNF & MIC) and gelatinous predators (Straile, 1997); 10%-30% for mesozooplankton (Anderson et al., 2018); 5% – 30% for bacteria (del Giorgio and Cole, 1998); and 50% – 90% AE for all heterotrophs (Conover, 1966).

Minimum respiration requirements were considered as both active respiration and basal respiration. Active respiration was set as a fraction of ingestion, and basal respiration was set as a function of biomass and temperature. Valid solutions fulfilled both criteria. Diel vertical migrator biomass, as determined from MOCNESS net tows, was used to calculate a minimum respiration based on temperature. DOC excretion was required to be greater than 10% of ingestion (or 2% of NPP for phytoplankton) and less than respiration (or 35% of NPP). All inequality constraints are listed in Supplemental Table 1.

284

2.2.2. Model solution

Because the LIEM is under-constrained, there are infinite possible solutions that satisfy the equality and inequality constraints. To choose a mean solution, and to determine uncertainty, within the possible solution space, we use a Markov Chain Monte Carlo (MCMC) sampling method (Kones et al., 2009; van den Meersche et al., 2009; van Oevelen et al., 2010), which has been shown to reconstruct unmeasured flows more accurately than the L_2 minimum norm approach (Saint-béat et al., 2013; Stukel et al., 2012, 2018a). Implementation details are provided in the online supplement.

As a metric for discussing model results with respect to the approximation equations (i.e. the observations), we use the model-observation misfit relative to the model uncertainty: $\Sigma = (X_{model} - X_{obs})/\sigma_{obs}$. Here X_{model} is the model prediction, X_{obs} is the observed value, and σ_{obs} is the standard deviation of the observed value. The square of this quantity (Σ^2) is summed over all approximate equations yielding the solution cost function, and thus Σ is a proxy for disagreement between the LIEM and observations. Unless otherwise stated, LIEM solutions will be given as a range based on the mean solution for each cycle as well as the median value of all cycles. Displaying data in this way allows us to highlight inter-cycle variability. For value and uncertainty in all rate constraints, see Appendix A.

11

302

2.3. Analyses and model comparisons

2.3.1. Indirect analysis

An indirect analysis permits investigation of the contributions of carbon between any two compartments through indirect linkages. By taking the normalized matrix of flows between compartments (G) and the identity matrix (I), the matrix (I-G)$^{-1}$ provides all the indirect flow data (Kroes, 1977). In this way the contribution of the surface compartments to the deep ones can be ascertained even when no direct flows exist. For example, if the food chain was A → B → C; an indirect analysis would reveal that 100% of the flows to C go through A.

2.3.2. Independent DVM estimates

A model to predict the export flux due to zooplankton DVM was recently published by Archibald et al. (2019), which adds a diel vertical migration module to the Siegel et al. (2014) ecosystem model. The Archibald et al. model parameterizes the export production based on NPP, size-fractionated grazing (i.e., protists and mesozooplankton), and the proportion of DVM mesozooplankton. The export production attributed to vertical migrators who defecate at depth is a function of total grazing, the gut clearance rate, and the proportion of zooplankton undergoing DVM (Eq. 2).

$$Export_{twilight} = p_{DVM} \cdot (1 - f_{fec}) \cdot \left(m_{fec} \cdot G_m + n_{fec} \cdot G_n \right) \tag{2}$$

Where p_{DVM} is the fraction of mesozooplankton that undergo DVM, and f_{fec} is the fraction of fecal pellets produced by diel vertical migrators in the euphotic zone. m_{fec} and n_{fec} are the proportions of grazing that are exported by mesozooplankton and protistan zooplankton, respectively. G_m and G_n are the grazing rates for mesozooplankton and protistan zooplankton, respectively.

The respiration conducted by vertically migrating zooplankton can be calculated based on the metabolic efficiency, fraction of mesozooplankton undergoing DVM, and their grazing rate (Eq. 3).

$$Export_{resp} = p_{met} \cdot p_{dvm} \cdot f_{met} \cdot \left[(1 - m_{fec}) \cdot G_m + \frac{n_{fec}}{m_{fec}} (1 - m_{fec}) \cdot G_n \right] \tag{3}$$

where p_{met} is the temperature dependent metabolic rate with ΔT the temperature difference between the mesopelagic and epipelagic and $p_{met} = 2^{(\Delta T/10)} / (2^{(\Delta T/10)} + 1)$. f_{met} is the metabolic efficiency of the zooplankton, assumed to be 0.50. We calculated active transport from Equations 3 and 4 following Archibald, but using the CCE-optimized parameter set that Stukel et al. (2015) determined for the Siegel et al. (2014) model. The fraction of mesozooplankton undergoing DVM (p_{dvm}) was calculated as described in Section 2.1.2. Fecal pellet production for meso- and microzooplankton were set to $m_{fec} = 0.3$ and $n_{fec} = 0.06$ (Archibald et al.,

336 2019), respectively.

337 Since the Archibald et al. model does not include mortality at depth as export and
338 excludes any mesopelagic ingestion or excretion, the total export flux is the sum of Eq. 2 and 3.
339 To compare with the LIEM presented here, a modified LIEM active transport flux will be
340 calculated using the total active transport for mesozooplankton and subtracting mesopelagic
341 mortality.

342

3. Results

3.1. *In situ* Ecosystem Observations

345 The locations for each study site were chosen to maximize the range of environmental
346 conditions (Figure 2). Sea surface chlorophyll a (Chl a) varied from 0.2 – 1.5 mg Chl a m^{-3} with
347 vertically-integrated primary productivity varying from 325 – 2314 mg C m^{-2} d^{-1}. Productivity
348 and biomass typically declined with distance from the Point Conception upwelling center. Most
349 cycles were in water masses with steady or declining phytoplankton biomass (Figure 2D), with
350 the exception of P0810-1. Sediment trap-derived carbon export at 100 m depth varied from 32 –
351 170 mg C m^{-2} d^{-1} (Figure 3C), with observed e-ratios (i.e. sediment trap export / ^{14}CPP) ranging
352 from 5% - 33%. Standing stock of zooplankton correlated positively with NPP and export
353 (Spearman correlations of 0.36 and 0.40, respectively). Protistan zooplankton were responsible
354 for grazing ~50% of NPP (Figure 3B) while mesozooplankton grazed, on average, ~30% of NPP
355 with one exception (Figure 3E). The proportion of mesozooplankton biomass exhibiting DVM
356 behavior ranged from 35% - 86% (median: 58%). Epipelagic bacterial production rates did not
357 correlate with NPP but ranged from 22 – 400 mg C m^{-2} d^{-1} (Figure 3F), with the three lowest
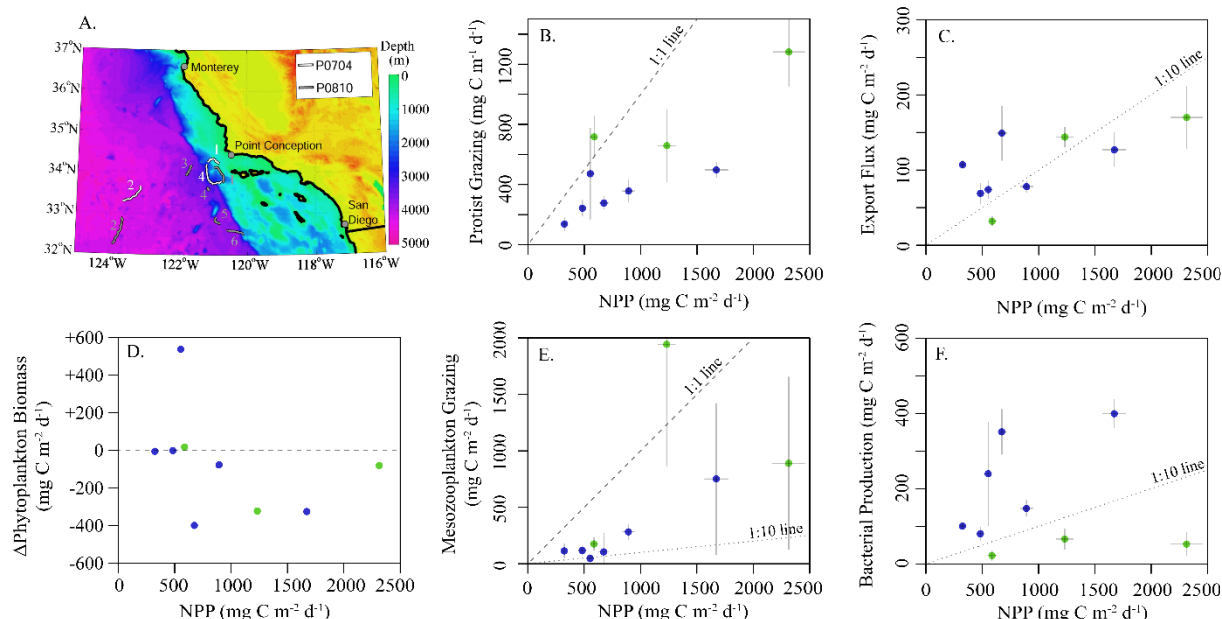358 rates observed during the P0704 Cruise.

359

13

Figure 2. A) Bathymetric map of study region showing drift trajectories from each cycle. Numbers correspond to cycle for P0704 (white) and P0810 (grey). (B-F) Summary of *in situ* observations plotted against NPP: (B) protistan grazing, (C) export flux from sediment trap at 100 m, (D) observed rate of change of phytoplankton biomass, (E) mean mesozooplankton grazing and (F) epipelagic bacterial production. Values are colored by cruise (P0704 = green, P0810 = blue). Dashed lines for reference slopes of 1:1, 1:10, or no change as indicated and error bars are ±1 SD.

3.2. Model-Observation Mismatch

The LIEM solutions consistently show general agreement with all *in situ* observations except for modeled NPP, which is elevated by 18% - 56% (median: 22%) from [14]CPP estimates (Figure 3A), or 3.0 – 9.3 Σ (median: 3.6 Σ). This degree of misfit corresponds to 18% – 82% (median: 46%) of the total model-observation misfit. Model agreement with the sediment trap was high (-33% – 25%; Figure 3E) with a modeled e-ratio (i.e. sediment trap export / NPP) of 5% – 35% (median: 14%), which compares well to the observed e-ratio of 5% – 33% (median: 11%). Modeled protistan grazing rates and mesozooplankton grazing rates were reasonably close to observations (Figure 3B). Modeled microzooplankton (MIC) grazing was lower than observed for cycles P0704-2 (-2.8 Σ) but agreed reasonably well (-1.5 – +0.1 Σ) for the other cycles (Supplemental Figure 1). For P0704-1, mesozooplankton grazing rates were lower than observations for SMZ (-1.8 Σ), total non-DVM grazing (-1.8 Σ) and for vmSMZ grazing (-1.6 Σ). This cycle exhibited declining phytoplankton biomass (-322 mg C m^{-2} d^{-1}) and very high zooplankton grazing rates compared to the other cycles. This water parcel may have been in a declining bloom stage where observed grazing rates were unsustainable. Model-data agreement among the seven nekton-related observations (e.g. Figure 3F) was satisfactory ($|\Sigma| < 1$) except for

14

378   P0810-1, which showed reduced vertically migrating nekton activity relative to estimates
379   (vmMYC epipelagic respiration: -1.5 Σ, vmMYC mesopelagic respiration: -1.7 Σ, and vmMYC
380   mesopelagic mortality: -1.1 Σ). This cycle was along the edge of an anti-cyclonic eddy, where
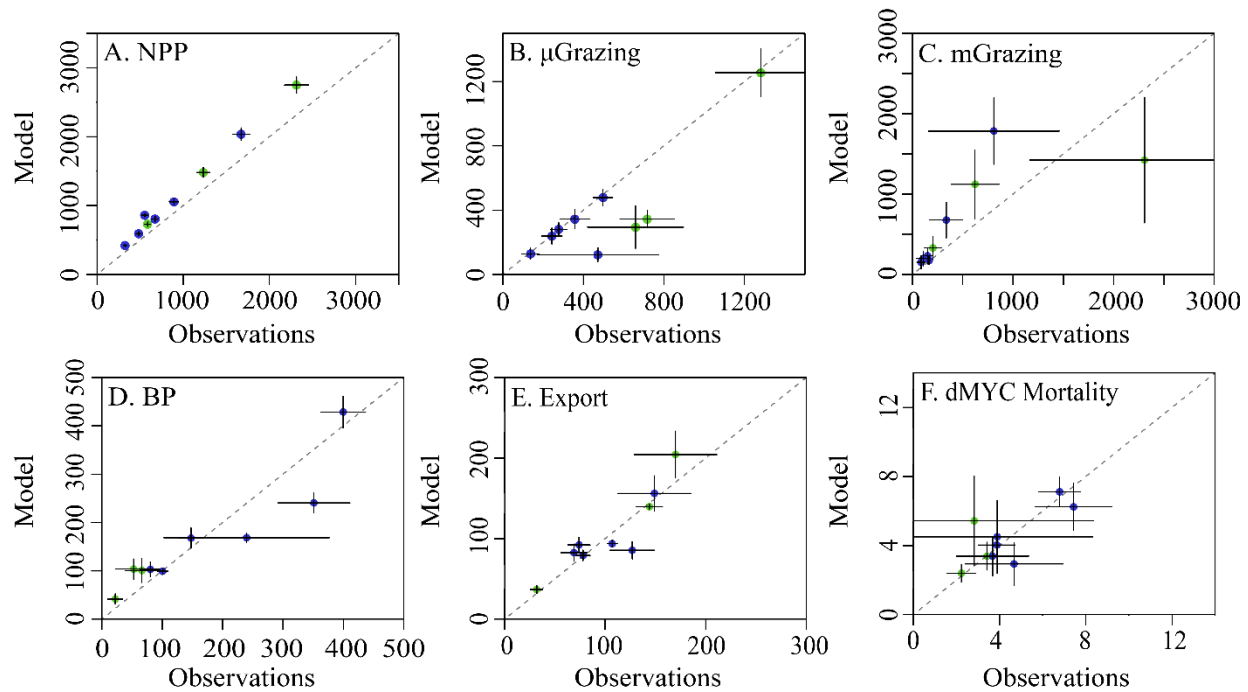381   lateral gradients were likely high.

382

383

Figure 3. Model-observation comparisons for selected measurements: (A) net primary
productivity, (B) protistan zooplankton grazing, (C) mesozooplankton grazing, (D) epipelagic
bacterial production, (E) sediment trap carbon export (@ 100m), and (F) non-vertically
migrating mesopelagic nekton mortality. Cruises are denoted by color (P0704 = green, P0810 =
blue). Dashed line is 1:1 and error bars show 1 SD of uncertainty.

389

3.3. Epipelagic Ecosystem Model

391   According to the LIEM, phytoplankton respired 18% - 39% (median: 30%) of GPP, lost
392   14% - 26% (median: 18%) as DOC, lost 2% - 42% (median: 6%) to non-grazer mortality and the
393   remaining 5% - 54% (median: 45%) was grazed by zooplankton. Modeled NPP ranged from 421
394   mg C m^{-2} d^{-1} to 2750 mg C m^{-2} d^{-1} (median: 861 mg C m^{-2} d^{-1}). The LIEM suggested that protists
395   and mesozooplankton had relatively similar grazing impacts on phytoplankton across all cycles,
396   although the proportional role was greater for mesozooplankton in coastal regions and greater for
397   protists during oligotrophic conditions. Between 14% and 47% (median: 33%) of NPP was
398   grazed by protistan zooplankton (MIC + HNF) and 18% - 96% (median: 45%) by
399   mesozooplankton (SMZ + vmSMZ + LMZ + vmLMZ). We note that protistan grazing rates

15

400   normalized to NPP are slightly depressed relative to observations since model NPP was higher

401   than observations while protistan grazing generally matched the observations (Figure 3;

402   Supplemental Figure 1). 57% - 82% (median: 74%) of mesozooplankton grazing was by small

403   mesozooplankton (SMZ + vmSMZ). Vertically migrating mesozooplankton were responsible for

404   52% - 89% (median: 63%) of total mesozooplankton grazing, 58% - 85% (median: 77%) of

405   which was done by small mesozooplankton (i.e. vmSMZ grazing / total vm grazing).

406   Mortality relative to ingestion for mesozooplankton was similar for the different

407   epipelagic mesozooplankton (i.e. SMZ, LMZ, vmSMZ, and vmLMZ): SMZ: 24% - 25%,

408   vmSMZ: 23% - 25%, LMZ: 22% - 25%, and vmLMZ: 24% - 27%, as was fecal pellet production

409   (between 30% and 40% of ingestion).

410   Overall, 19% - 44% (median: 29%) of NPP was transferred from the epipelagic to the

411   mesopelagic with 3% - 8% (median: 5%) of NPP leaving the epipelagic through higher trophic

412   levels (SAR + vmMYC). Gravitational settling and subduction of POC accounted for 14% - 78%

413   (median: 55%) of epipelagic export, while 18% - 84% (median: 41%) was through active

414   transport of DVM mesozooplankton (vmSMZ + vmLMZ). Vertically migrating myctophids

415   (vmMYC) transferred 2% - 6% (median: 4%) of total export. Section 3.4 provides a more

416   detailed description of export production.
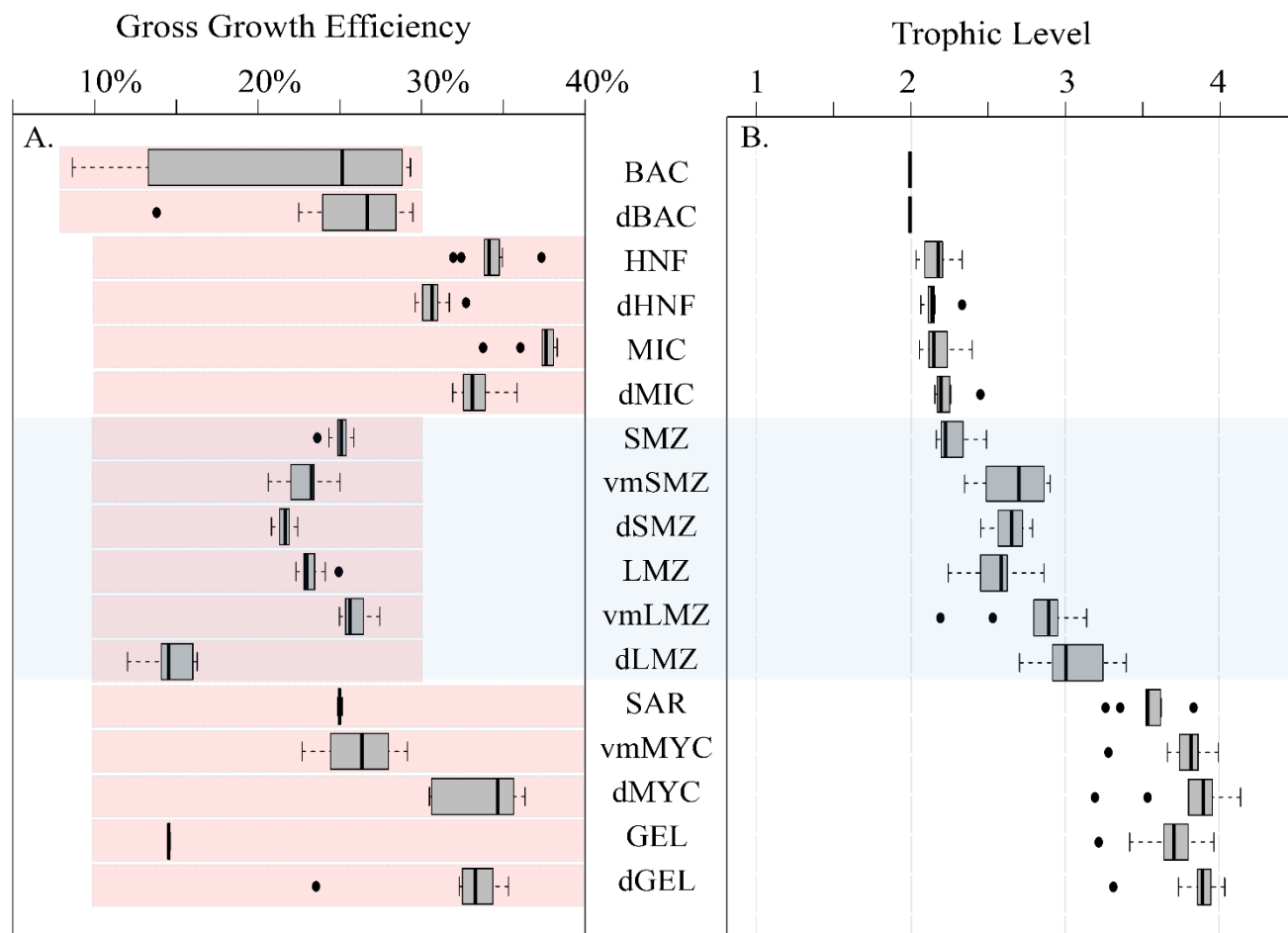
417

418

16

Figure 4. (A) Box and whisker plot of GGE for organisms in the LIEM. Red shaded boxes indicate the permitted range of values constraining the LIEM. (B) Box and whisker plot of trophic levels for each zooplankton assuming detritus and primary productivity are trophic level 1, and bacteria are trophic level 2. Box and whisker plots show inter-quartile range and 95% C.I. as determined using the mean solutions for each cycle. For reference the mesozooplankton compartments are shaded across both figures. Abbreviations are explained in Table 2.

The gross growth efficiencies (GGE) for each type of organism are shown in figure 4A. Overall, BAC GGE was 7% - 29% (median: 25%) with an upper bound set to 30%. Notably, BAC GGE differed based on cruise, with P0704 cycles ranging between 8% - 13% and P0810 ranging between 23% - 29%. MIC GGE was 35% - 38% (median: 37%), and HNF GGE ranged from 32% - 35% (median: 33%), which is slightly higher than typical estimates of protistan zooplankton GGE (Straile, 1997) although reported variability is high (Steinberg and Landry, 2017). Epipelagic mesozooplankton GGE were consistently above 20%.

3.3.1 Trophic Level & Diets

17

436   Trophic levels for each organism (Figure 4B) were calculated by assuming that primary
437   productivity, detritus and DOC were at trophic level 1. Trophic level indices were not affected
438   by the overall cycle productivity (i.e. NPP), time of year, or by nutrient regime. The trophic level
439   of small epipelagic mesozooplankton (SMZ) ranged from 2.2 to 2.5 (median: 2.2) and large
440   mesozooplankton (LMZ) ranged from 2.2 to 2.9 (median: 2.6). The SAR trophic level was 3.3 –
441   3.8 (median: 3.5), and vmMYC was similar at 3.3 – 4.0 (median: 3.8). Modeling these higher
442   trophic levels is important for structuring the ecosystem, and the nekton trophic levels found here
443   are consistent with findings from ^{15}N amino acid studies (Choy et al., 2015).

444   The modeled mesozooplankton ingestion can be classified into four distinct dietary types:
445   (1) Herbivory = phytoplankton diet, (2) Protistivory = protistan zooplankton diet, (3) Detritivory
446   = detrital diet (i.e. SDT or LDT), and (4) Carnivory = mesozooplankton diet. Using this
447   partitioning, the relative contributions of each dietary component were assessed for large and
448   small vertically migrating mesozooplankton compartments (Figure 5). The largest proportion of
449   the diet for resident epipelagic mesozooplankton (i.e. SMZ & LMZ) was balanced between
450   herbivory (19% - 57% median: 40%) and protistivory (26% - 59% median: 40%). Detritivory
451   was 9% - 21% (median: 13%) of total diet. Inter-cycle variability in carnivory was low for
452   resident epipelagic mesozooplankton and contributed 6% - 8% (median: 6%) of their diet.

453   Comparing the LIEM solutions between the nutrient limited and upwelling cycles, we
454   found that large mesozooplankton grazing increased from 9% - 16% (median: 13%) in the
455   nutrient limited cycles to 22% - 65% under upwelling conditions (median: 30%) of NPP,
456   although the overall diets of the mesozooplankton did not systematically change with nutrient
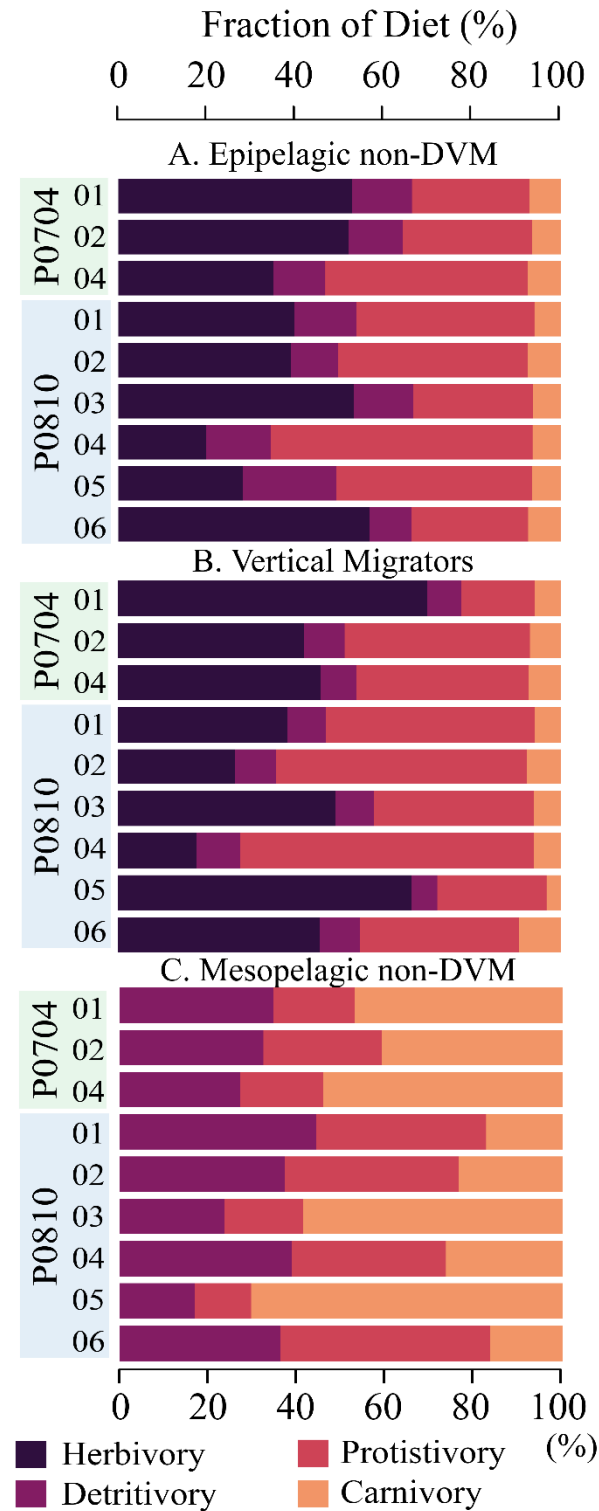457   condition.

458

18

Figure 5. Composition of diet for (A) epipelagic, non-DVM mesozooplankton, (B) vertically migrating mesozooplankton, and (C) mesopelagic, non-DVM mesozooplankton. Diet is partitioned into herbivory (darkest), protistivory, detritivory, and carnivory (lightest). Cycles are as indicated.

464

3.4. New Production, Export and DVM

466   Total export ranged from 163 - 707 mg C m^{-2} d^{-1} (median: 282 mg C m^{-2} d^{-1}) with
467   distinctly elevated values associated with upwelling cycles (Figure 6A). The fraction of export
468   attributed to mesozooplankton DVM (vmSMZ + vmLMZ) covaried with nutrient regime:
469   mesozooplankton active transport contributed 14% - 37% of total export under nutrient limited
470   conditions and 44% - 84% under upwelling conditions (Figure 6B). There was not a significant
471   relationship (p < 0.1) between the total export efficiency (i.e. total export / NPP) and NPP
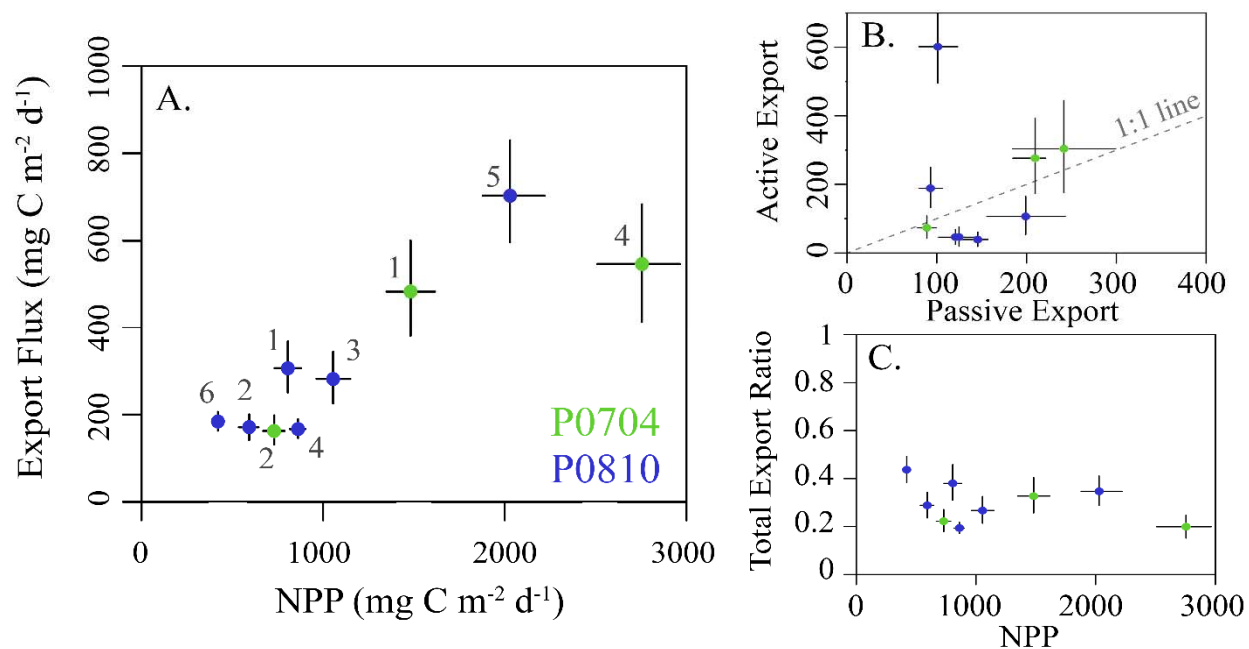472   (Figure 6C).

473

475   **Figure 6**. (A) The sum of both passive and active carbon export flux from the epipelagic plotted
476   against NPP. Cruises are color coded and error bars show the 95% CI for each value. (B) The
477   total active flux due to DVM verses passive flux for each cycle (as in A). Dashed 1:1 line for
478   reference. (C) The total export ratio (i.e. total epipelagic export / NPP) plotted against NPP and
479   colored as in (A). All values are in mg C m^{-2} d^{-1}.

480

481   For vmSMZ, 77% - 80% (median: 80%) of their respiration took place in the epipelagic,
482   along with 67% - 87% (median: 85%) of their DOC excretion. This is consistent with the
483   suggestion that mesozooplankton respiration and excretion are elevated in the warmer epipelagic
484   waters (Ikeda, 1985) and where activity is highest.

485   The fate of active export flux is important for understanding the ecological impact of this

carbon supply. Within the mesopelagic, mesozooplankton respired 11 – 104 mg C m^{-2} d^{-1} (median: 33 mg C m^{-2} d^{-1}) and excreted 7 – 116 mg C m^{-2} d^{-1} (median: 20 mg C m^{-2} d^{-1}; Figure 7A). Predation on vertically migrating mesozooplankton accounted for a loss of 23 – 352 mg C m^{-2} d^{-1} (median: 59 mg C m^{-2} d^{-1}) in the mesopelagic. Mesozooplankton fecal pellet production in the mesopelagic was 8 – 29 mg C m^{-2} d^{-1} (median: 13 mg C m^{-2} d^{-1}). Resident mesopelagic mesozooplankton were the dominant mortality term for the vertically migrating mesozooplankton (Figure 7B).
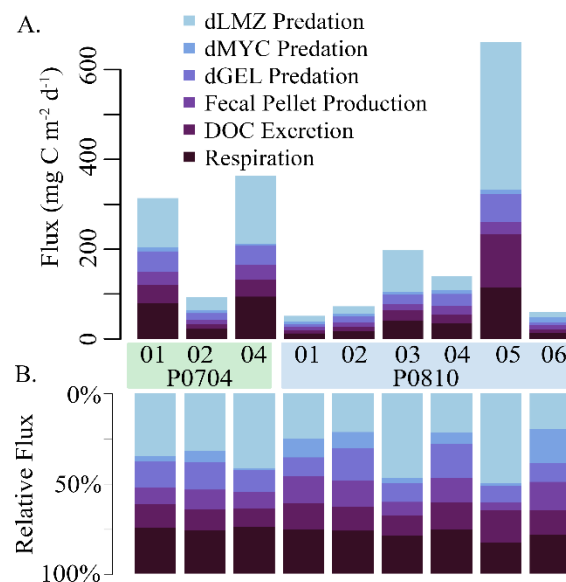

Figure 7. *The (A) net and (B) relative fate of vertically migrating mesozooplankton within the mesopelagic.* Loss terms are color coded, and cruise and cycle are as shown. Abbreviations are explained in Table 2.

3.5. Mesopelagic Ecosystem

Deep bacteria (dBAC) made up 6% - 30% (median: 11%) of the mesopelagic protistan zooplankton diet with the remainder supplied by detritus/fecal pellets. Mesopelagic mesozooplankton (i.e. dSMZ & dLMZ) had a more variable diet than the epipelagic mesozooplankton (Figure 5), with detritivory ranging from 17% - 43% (median: 39%) of their diet, protistivory at 14% - 51% (median: 30%) and carnivory at 10% - 68% (median: 33%).

Systematic increases in trophic level between the epipelagic and mesopelagic resident zooplankton and nekton were observed (Figure 4). The trophic level of epipelagic microzooplankton (MIC) was 2.0 – 2.3 while dMIC was 2.3 – 2.5. Similar increases between the epipelagic and mesopelagic were observed for mesozooplankton, where SMZ had a trophic level

21

506 of 2.2 – 2.5 (median: 2.2) dSMZ had a trophic level of 2.5 - 2.8 (median: 2.6). Likewise, dLMZ
507 trophic levels were elevated by ~0.4 relative to LMZ. The trophic level of dMYC (3.2 – 4.1) was
508 more variable than the other micronekton (e.g. vmMYC: 3.5 – 4.0), illustrating a greater
509 variability in diet.

510 　　　Mesopelagic respiration is a useful diagnostic loss term for determining which organisms
511 are responsible for the mesopelagic carbon demand (Supplemental Figure 2). Mesopelagic
512 bacteria accounted for the largest proportion of mesopelagic respiration (31%-41% median:
513 34%). High respiratory term for mesopelagic bacteria was found despite relatively high GGE for
514 these organisms (median 26%, Figure 4A). Mesopelagic protistan zooplankton and resident
515 mesozooplankton were responsible for 14% - 30% (median: 25%) and 14% - 24% (median:
516 15%), respectively. Resident gelatinous predators and myctophids are responsible for 4% - 8% of
517 mesopelagic respiration combined. The proportion of export due to active transport covaried
518 with resident mesopelagic respiration (Figure 8A), illustrating the coupling between active
519 transport and mesopelagic activity in the LIEM. The effect of higher active transport relative to
520 total export can be shown with an indirect analysis where the relative contribution of carbon
521 from epipelagic detritus (i.e., a passive transport proxy) and vertically migrating
522 mesozooplankton (i.e., an active transport proxy) in the diet of each organism can be measured.
523 Indirect flux analyses show that a higher proportion of the carbon consumed by mesopelagic
524 bacteria, protists, and mesozooplankton originated from passive rather than active transport
525 (Figure 8B). However, mesopelagic nekton (dMYC) were predominantly supported by carbon
526 derived from active transport pathways.

527
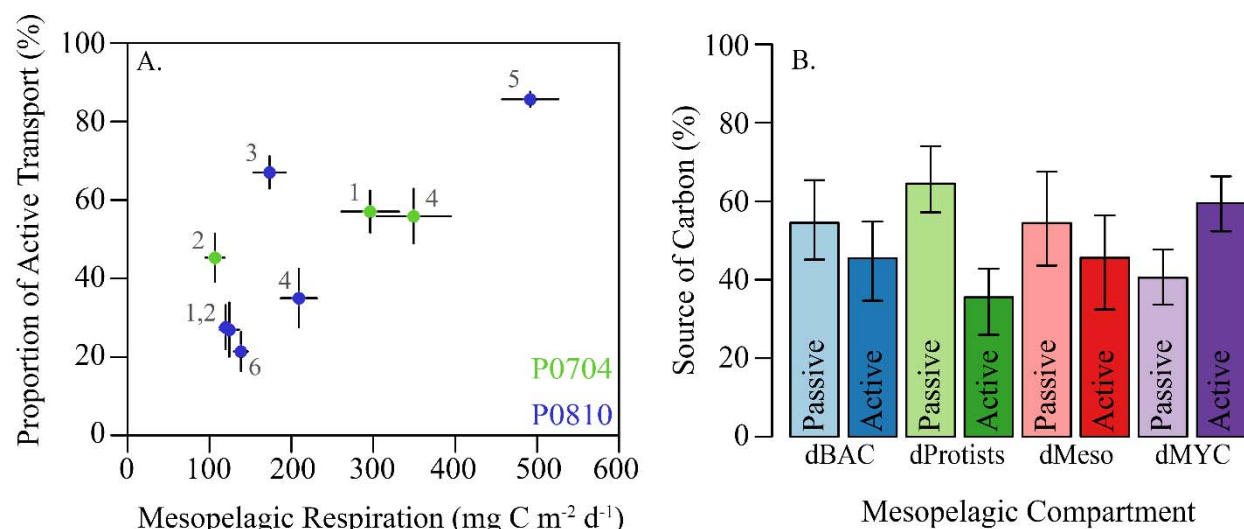

529 **Figure 8**. (A) Proportion of active transport relative to total export verses total mesopelagic
530 respiration by residents (i.e. dBAC, dHNF, dMIC, dSMZ, dLMZ, dMYC, dGEL). Cruises are
531 colored and cycles are as shown. (B) Relative proportions of carbon demand supplied by passive
532 or active flux for the indicated mesopelagic groups. Source was calculated using indirect flux

22

533   analysis (Section 2.3.1) to determine the indirect contribution epipelagic detritus (passive) and
534   vertically migrating mesozooplankton (active). Error bars are ±1 SD.

535

536   # 4. Discussion
537   ## 4.1. Diel Vertical Migration & Active Transport in the CCE

538   In contrast to common assumption about the processes driving the biological pump, our
539   results suggest that active transport may be as, if not more, important than sinking particle flux.
540   We found that active transport (mesozooplankton and fish combined) was responsible for 39 -
541   606 mg C m^{-2} d^{-1} (median: 107 mg C m^{-2} d^{-1}), corresponding to 21% - 86% of total export to the
542   mesopelagic, while sinking particles contributed 14% - 79%. This finding is not directly forced
543   by an *a priori* assumption of the importance of active transport. Indeed, we placed no direct
544   constraint on the amount of mesozooplankton mortality in the mesopelagic, and the minimum
545   constraints on basal metabolism by zooplankton in the mesopelagic (Stukel et al., 2013) implied
546   that active transport could have been as low as 2% – 40% of sinking flux (median: 18%).
547   Nevertheless, the importance of active transport was a robust result of the inverse analyses. For
548   P0810-6, the cycle with the lowest relative contribution of active transport to total export (21%),
549   the total flux was 184 ± 23 mg C m^{-2} d^{-1} (95% CI) and active transport was 39 ± 21 mg C m^{-2} d^{-1}
550   (95% CI). This cycle was oligotrophic and had the lowest ^{14}CPP measurements of any cycle on
551   the two cruises. In contrast, cycle P0810-5 had the highest relative contribution of active
552   transport (86% ± 4% of total export at the 95% CI). P0810-5 was on the coastal (i.e. high
553   biomass) side of a strong frontal feature with high rates of primary productivity and large
554   standing stocks of zooplankton.
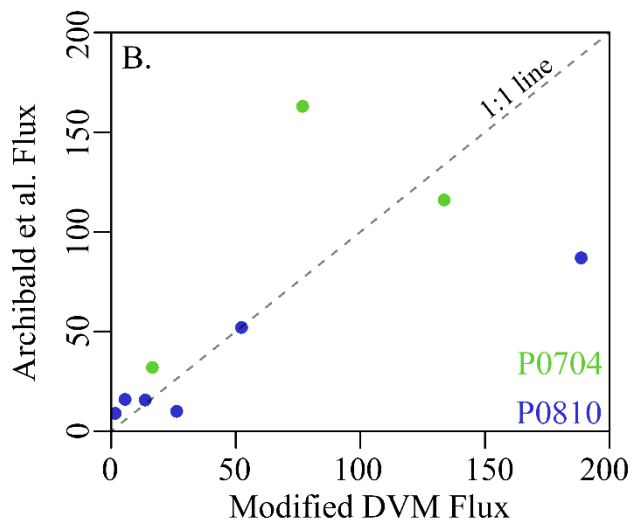
555

556

Figure 9. Comparison between modeled mesozooplankton DVM flux without mesopelagic
mortality and the predicted flux from Archibald et al. (2019) with CCE-specific parameterization

23

559   following Stukel et al. (2015). Cruises are as colored (P0704 = green, P0810 = blue) and dashed
560   line is a 1:1 reference line. Fluxes are shown in mg C m^{-2} d^{-1}.

561

562   Although these rates of active transport are higher than reported in many studies, they are
563   fully consistent with mesozooplankton community dynamics in the CCE. The model suggests
564   that total epipelagic mesozooplankton consumption on phytoplankton, protists, detritus, and
565   other mesozooplankton ranged from 361 - 2966 mg C m^{-2} d^{-1} (median: 1006 mg C m^{-2} d^{-1}).
566   Vertically stratified day-night net tows showed that 35% - 86% (median: 57%) of the
567   mesozooplankton community was vertically migrating to depth each day and that most of these
568   vertical migrants were copepods and euphausiids (Stukel et al., 2013). Our model results indicate
569   that only 20% - 23% of respiration and 16% - 34% of excretion by vertical migrants occurred at
570   depth. None of these assumptions are particularly aggressive. Furthermore, our results (Figure 9)
571   are consistent with estimates of DVM in the zooplankton derived from the model of Archibald et
572   al. (2019), if specific dynamics of the CCE are taken into account (e.g., zooplankton consume
573   nearly all of NPP, Landry et al. 2009; microphytoplankton are negligible contributors to sinking
574   flux, Stukel et al. 2013). Our estimates of the total export ratio 19% - 44% are also consistent
575   with typical *f*-ratio estimates (new production to total export) in our study region, which varied
576   from 0.23 to 0.40 (Krause et al., 2015). Our results thus do not arise from unusual
577   parameterizations but instead may reflect the fact that estimates of active export using standard
578   metabolism calculated from Ikeda et al. (1985; 2001) may be conservative underestimates.

579   Our results also reflect realistic coupling between the epipelagic and mesopelagic
580   communities. Model results suggested that the carbon demand was equal to <1% - 4% (median:
581   1.1%) of NPP for mesopelagic fish, 1% - 7% (median: 3%) of NPP for predatory gelatinous
582   zooplankton, 8% - 22% (median: 14%) of NPP for resident mesopelagic zooplankton, and 6% -
583   19% (median: 11%) of NPP for mesopelagic bacteria. These mesopelagic carbon demands must
584   be met by carbon flux from the surface layer, the most likely sources of which are sinking
585   particle flux (which we experimentally measured using two independent approaches) and active
586   transport. While it is possible that both sediment traps and ^{238}U-^{234}Th disequilibrium
587   underestimated sinking carbon flux, the inverse analysis offers compelling evidence that active
588   transport is more likely to support mesopelagic fish and gelatinous predator communities.
589   Although sinking particles can efficiently support bacterial production (as they are likely directly
590   colonized by particle-attached bacteria), many fish and gelatinous zooplankton are predators that
591   more likely feed on living organisms than on the sinking fecal pellets that typically dominate
592   particle flux in the CCE. For these planktivorous organisms, sustaining their metabolism through
593   a food chain supported by sinking particles would likely require one (if not more) trophic levels
594   to separate them from the export source, depending on whether the sinking particles are
595   consumed by filter- or flux-feeding zooplankton or by microbes (Stukel et al., this issue). Thus,
596   sustaining the high carbon demand of mesopelagic myctophids with sinking particles requires
597   substantially more total carbon flux than does sustaining it via active transport of the

24

598   myctophids' prey.

599   Mesopelagic sources of mortality have implications for the fitness of vertical migrators. It
600   is often assumed that DVM is ecologically advantageous when the costs associated with not
601   feeding during the day and actively swimming to depth are offset by the benefits of reduced
602   predation pressure and/or reduced metabolism at colder mesopelagic temperatures (Bianchi et
603   al., 2013; Hansen and Visser, 2016; Morozov and Kuzenkov, 2016). Our model suggests that
604   mortality normalized to ingestion is similar across all mesozooplankton compartments and across
605   a wide range of ecosystem states (SMZ: 24% - 26%, LMZ: 22% - 25%, vmSMZ: 21% - 25%,
606   vmLMZ: 25% - 27%, dSMZ: 21% - 23%, dLMZ: 19% - 23%). Even though vmSMZ experience
607   similar predation to SMZ and dSMZ, approximately half of the predation on vertically migrating
608   zooplankton takes place in the mesopelagic, thereby transferring carbon to depth despite the fact
609   that their excretion and respiration occur primarily in the epipelagic.

610   The comparable mortality experienced by vertically-migrating mesozooplankton in the
611   mesozooplankton may seem counterintuitive in light of extensive research suggesting that the
612   adaptive advantage of DVM may be to reduce predation (Bandara et al., 2018; Ohman and
613   Romagnan, 2016). However in the CCE, it is not particularly surprising when the large
614   abundances of myctophids, gonostomatids, and other mesopelagic fish are considered. Davison
615   et al. (2013, 2015) demonstrated high biomass of these fish comprising both vertically-migrating
616   and mesopelagic resident communities. These organisms may thus face as high, if not higher,
617   predator abundance at mesopelagic depths than in the epipelagic, although colder temperatures
618   and reduced irradiance may diminish predation rates at depth. DVM may remain advantageous
619   as a lifestyle because if these organisms were present at the surface during the day then they
620   might experience substantially greater predation than in the mesopelagic.

621

4.2. Sensitivity Analysis and Ecological Connections

623   The ecosystems generated in the 9 model runs were as varied as the cruise measurements:
624   including observations from dynamic coastal blooms to quiescent oligotrophic communities. All
625   9 cycles had significantly elevated NPP compared to the observed [14]CPP (Figure 3;
626   Supplemental Figure 1) with 95% CI from the MCMC random walk. Whether this result can be
627   considered a model bias or is derived from possible systematic differences between [14]CPP and
628   true net primary production (Marra, 2009; Milligan et al., 2014; Minas et al., 2002; Peterson,
629   1980) is not known. To test the model's sensitivity to the misfit with [14]CPP, the LIEM was rerun
630   assuming that [14]CPP uncertainty was 1/10th of the actual estimated uncertainty. The model-
631   observation misfit increased by nearly 2.5x with small mesozooplankton grazing rates,
632   myctophid metabolic estimates, and sediment trap export all reduced by ~2 Σ relative to the
633   standard model run. This result shows that the model needed to increase NPP in the standard
634   model run in order to match the observed mesozooplankton grazing rate and myctophid
635   metabolic requirements.

636   Because bacterial activity in the mesopelagic was not measured we made conservative
637   assumptions about the possible upper and lower bounds for bacterial production. For the
638   minimum bound on mesopelagic BP, we chose a conservative power-fit slope of -1.47
639   (Yokokawa et al., 2013). This resulted in model-determined mesopelagic bacterial carbon
640   demand that may have been lower than true *in situ* values. Other reported values for the
641   attenuation of BP in the mesopelagic include slopes of $\alpha = 1.15$ (Tanaka and Rassoulzadegan,
642   2004) and 1.03 (Gasol et al., 2009), which would result in 25% and 36% higher estimates of
643   mesopelagic BP, respectively. When the minimum mesopelagic bacterial production estimates
644   were doubled ($\alpha = 0.64$; Eq. 1), the model responded by increasing NPP by +2% (inter-cycle
645   median) and total export flux by 11%. Since passive particle flux is constrained by observations,
646   passive flux increased by 0% - 12% (median: 4%) while active transport by mesozooplankton
647   increased by 0% - 56% (median: 26%). Active transport by nekton was also elevated (0% - 14%,
648   median: 10%). Model-observation misfit increased by an average of 17% with notable changes
649   in NPP (+0.42 Σ), sediment trap flux (+0.34 Σ) and Thorium-234 flux (+0.22 Σ).

650   The results were also robust to changes in other observations. When the nekton metabolic
651   estimates were halved, export by vmMYC was reduced by 51% (inter-cycle median), a change of
652   < 5 mg C m^{-2} d$^{-1,}$ while other forms of export were unchanged. Increasing the upper limit of
653   mesozooplankton GGE from 30% to 40% led to a ~20% increase in mesozooplankton active
654   transport and no change in nekton-derived active flux or passive flux.

655

4.3. Linear Inverse Models

657   LIEMs are a powerful tool for assimilating diverse *in situ* measurements and constraints
658   with a food web perspective. The use of a two-layer model (Jackson and Eldridge, 1992) is
659   particularly powerful because it allows information from the mesopelagic to constrain epipelagic
660   food web flows and vice versa. Compared to most previously published LIEMs, the model
661   presented here includes many more *in situ* rate measurements, made possible by the suite of
662   contemporaneous rate measurements made during quasi-Lagrangian experiments. For
663   comparison, many LIEMs are constrained by fewer rate measurements (Dubois et al., 2012;
664   Sailley et al., 2013; van Oevelen et al., 2012) and therefore rely much more heavily on greater
665   than/less than constraints derived from biomass measurements, leading to correspondingly
666   higher uncertainty. This highlights a need for studies that simultaneously quantify the activity of
667   many different plankton functional groups.

668   Since a LIEM is fundamentally a data-regression technique, our results are emergent from
669   (A) our observations, (B) the conservative assumptions used (e.g. GGE), and (C) the ecosystem
670   structure. Thus, we believe the resulting model solutions to be descriptive of the dominant *in situ*
671   processes in the CCE LTER study region. However, it is important to note that there was large
672   uncertainty associated with some model flows, and that this uncertainty could be quantified using
673   the MCMC approach (Supp. Table 2). We thus highly recommend the MCMC approach (Kones

26

674 et al., 2009; van den Meersche et al., 2009), which has been shown to more robust in its ability to
675 recover ecosystem rates (Saint-béat et al., 2013; Stukel et al., 2012). Even more important is its
676 ability to generate confidence intervals that realistically represent the uncertainties in model
677 outputs with respect to both measurements and under-determinacy of the model. For instance, on
678 cycle P0810-6, we found that the 95% confidence interval for HNF ingestion of detritus was 5 -
679 127 mg C m^{-2} d^{-1}, providing no real knowledge of whether or not this connection was an
680 important part of the ecosystem. However, for Cycle P0810-5, we found that mesopelagic
681 mesozooplankton predation on small vertical migrators was 233 - 423 mg C m^{-2} d^{-1} (95% CI) and
682 hence have a high degree of confidence that this flow was substantial at this location.
683 Investigation of the confidence intervals can thus inform which conclusions can be considered
684 robust. Developing even better-resolved ecosystem models likely requires incorporation of more
685 diverse measurement types, such as ^{15}N isotopic data (Stukel et al., 2018a).

686

687 **4.4. The biological carbon pump and mesopelagic flux attenuation**

688 Reports of active transport by vertically migrating biota have long suggested that these
689 organisms can transport a globally significant amount of carbon to depth. However, most early
690 studies suggested that active transport was substantially less important than passive flux of
691 sinking particles (Davison et al., 2013; Morales, 1999; Steinberg and Landry, 2017). At the
692 oligotrophic BATS station off Bermuda, Dam et al. (1995) found that respiration by
693 mesozooplankton augmented the passive carbon flux at 150 m by 18% – 70%. Also at BATS,
694 Steinberg et al. (2000) reported a significant vertical transfer of nitrogen by zooplankton,
695 including dissolved organic nitrogen (DON). In fact, vertical migrators were found to perform
696 15% - 66% of the total nitrogen transport. Hansen and Visser (2016) estimated that across the
697 North Atlantic active transport by mesozooplankton may constitute 27% of total export. In
698 addition to zooplankton, vertical migrations by micronekton can also lead to significant export
699 fluxes (Angel and Pugh, 2010; Davison et al., 2013; Hernandez-Leon et al.). Using biomass
700 estimates and metabolic relationships, Davison et al. (2013) found micronekton contributions of
701 22 – 24 mg C m^{-2} d^{-1} (or 15% - 17% of estimated passive export) in the northeast Pacific. In the
702 North Pacific Subtropical Gyre, Al-Mutairi and Landry (2001) estimated that active transport
703 due to zooplankton respiration was responsible for carbon flux equal to 18% of passive flux.
704 Using a conservative approach, Longhurst (1990) estimated that active export by zooplankton
705 DVM was 13% - 58% that of passive flux when accounting for respiration alone in subtropical
706 waters, which is similar to our results where the LIEM suggests that mesozooplankton
707 respiration at depth is 9% – 113% (median: 34%) that of passive export. Global modeling
708 estimates have suggested that active transport may be responsible for 14% (Archibald et al.,
709 2019) or 15 to 40% (Bianchi et al., 2013) increases in carbon export relative to sinking particles
710 alone. More recent results, have been suggesting increased importance for active transport,
711 potentially rivaling that of passive flux. In the Costa Rica Dome, a region with high
712 mesozooplankton biomass like the CCE, Stukel et al. (2018b) identified active transport by

713   zooplankton DVM as responsible for 21-45% of total euphotic zone export. Hernández-León et

714   al. (this issue) found that active transport was equal to one quarter of passive flux in oligotrophic

715   regions, but was 2-fold higher than passive flux in eutrophic areas of the tropical and subtropical

716   Atlantic. Our results that total active transport (zooplankton and nekton) may be responsible for

717   18% - 84% (median: 42%) of total carbon export in the CCE are thus somewhat higher than

718   found in most studies, but not consistent with recently published values for high zooplankton

719   biomass regions. Furthermore, our results are in line with other biogeochemical and ecological

720   expectations (e.g., mesopelagic carbon demand, euphotic zone new production,

721   mesozooplankton energy partitions). We thus suggest that active transport in high biomass

722   regions may be more important, in fact, than some previous studies suggest, and we recommend

723   focused research to investigate the potentially conservative assumptions made in previous studies

724   that rely on standard (rather than active) estimates of zooplankton metabolic rates.

725   Within the mesopelagic, zooplankton also play an important biogeochemical role in the

726   attenuation of particle flux (Buesseler and Boyd, 2009; Steinberg et al., 2008; Stukel et al., this

727   issue) and in effecting elemental cycling (Kiko et al., this issue; Robinson et al., 2010). Our

728   results suggest that mesozooplankton detritivory accounted for the consumption of 57% - 71% of

729   sinking particles from the epipelagic, with bacterially-mediated remineralization of the majority

730   of the remainder (i.e. mesopelagic export efficiency is < 10%). Notably, 3 of the 4 cycles with

731   the lowest proportion of detritivory and the largest proportion of carnivory in the resident

732   mesopelagic zooplankton were during upwelling cycles. This is the opposite of the findings of

733   Wilson et al. (2010), who observed increases in fatty-acid biomarkers associated with carnivory

734   at station Aloha relative to K2 and attributed the increase to the lower primary productivity at

735   station Aloha. Our result that zooplankton rely more heavily on carnivory in the mesopelagic

736   agrees with fecal pellet characteristic analyses and fatty acid biomarkers measured by Wilson et

737   al. (2008) and Wilson et al. (2010), respectively. However, given the advective nature of an

738   eastern boundary current and frequency of non-steady state conditions, it is difficult to generalize

739   from our results to the rest of the Pacific. Clearly additional studies are necessary.

740   Since direct *in situ* measurements of subducted flux remains a technical challenge

741   (Bishop et al., 2004; Omand et al., 2015), few models have attempted to explicitly include

742   subducted POC into the carbon budget. Here we incorporated estimates of subducted flux for all

743   9 cycles based on results from a data-assimilative, Lagrangian particle study (Stukel et al.,

744   2018c). By placing constraints on the subduction of POC to depth, we were better able to

745   constrain the role of mesozooplankton in export production.

746

5. Conclusions

748   The LIEM used here incorporated numerous *in situ* measurements made during quasi-

749   Lagrangian experiments in the CCE in order to constrain carbon flows through the ecosystem.

750   These observations were made in water parcels spanning a wide range of conditions from highly

751   productive upwelling regions to an oligotrophic offshore domain and consistently found that

752   active transport of carbon by mesozooplankton was important to supplying the mesopelagic

753   carbon demand. Our results suggest that passive POC flux—i.e. the portion of flux that is often

754   assumed to dominate the biological pump—contributed 14% - 78% (median: 54%) of carbon

755   flux. This finding has implications for the interpretation of sediment trap and ^{234}Th

756   disequilibrium measurements and for helping to reconcile a long-studied imbalance in the

757   observed mesopelagic carbon budget. The LIEM also highlights the central importance of

758   zooplankton in marine food webs and biogeochemistry. Excretion by vertical migrants is

759   important in meeting bacterial carbon demand, while predation on vertical migrants supports

760   mesopelagic resident fish communities. Our analysis comprises a unique, fully-resolved

761   phytoplankton-to-fish coupled food web of the epipelagic and mesopelagic ocean. Nevertheless,

762   substantial uncertainties remain, and targeted studies are necessary to validate the suggested

763   relationships *in situ* and to test their applicability across the global ocean.

764

765 **Appendix A**

766 **Table A1**. Measurement constraints used in the LIEM. Values given show the mean (μ) and 1 SD (σ) for each cycle except for
767 min/max constraints which are blank. Marked values (*) were assumed values calculated from cycles of the same classification (see
768 Section 2.1.2). All values are given in mg C m^{-2} d^{-1}.

	Quantity	P07.1		P0704-2		P0704-4		P0810-1		P0810-2		P0810-3		P0810-4		P0810-5		P0810-6	
		μ	σ	μ	σ	μ	σ	μ	σ	μ	σ	μ	σ	μ	σ	μ	σ	μ	σ
1	C-14PP	1233	74	587	35	2314	139	554	33	484	29	893	54	674	40	1672	100	325	19
2	Delta PHY	-322	209	18	253	-80	602	538	1680	-1	50	-76	166	-399	4771	-325	173	-5	62
3	Microzooplankton Grazing	659	238	717	135	1282	225	472	301	243	51	357	74	277	41	498	48	138	43
4	SMZ Grazing	2249	1132	123	37	856	652	21	9	90	26	199	53	48*	21*	836*	688*	85*	37*
5	LMZ Grazing	93	87	42	18	123	55	18	12	14	9	66	26	21*	15*	51*	55*	19*	14*
6	vmSMZ Grazing	2092	907	137	44	669	499	50	30	110	34	249	113	72*	50*	753*	538*	101*	47*
7	vmLMZ Grazing	232	171	42	18	132	42	19	11	20	10	51	25	19*	14*	95*	101*	22*	16*
8	SMZ + LMZ Grazing	2342	1077	166	57	979	763	35	31	104	44	265	65	67*	38*	887*	668*	104*	61*
9	Total MesoZ Grazing	2306	1137	203	82	622	238	86	42	165	11	336	163	107*	70*	809*	650*	150*	41*
10	Sed Trap @ 100m	144	13	32	6	170	41	74	11	69	13	78	7	149	36	127	22	107	5
11	Thorium @ 100m	77	11	32	10	121	45	32	60	51	29	18	22	46	38	53	13	54	8
12	Fecal Pellet Flux @ 100m	135		4		54		4		8		5		35		14		4	
13	Minimum Subduction	39		47		25		11		33		13		26		10		31	
14	Maximum Subduction	79		55		45		33		47		15		51		19		59	
15	Epi Bacterial Prod (0-100m)	66	27	22	12	53	30	240	137	80	17	148	21	351	60	400	37	101	8
16	Min dBAC BP	16		5		8		16		13		14		27		102		21	
17	Max dBAC BP	52		16		27		52		41		45		89		336		69	
18	Deep NM Resp (dMYC)	2.8	5.5	3.4	1.0	2.2	0.7	4.6	2.2	3.6	1.7	3.8	0.8	3.8	4.4	6.7	0.9	7.3	1.8
19	Deep NM Poop (dMYC)	1.2	2.4	1.5	0.5	1.0	0.3	2.1	1.0	1.6	0.7	1.7	0.4	1.7	1.9	3.0	0.4	3.3	0.8
20	Deep NM Mort (dMYC)	2.8	5.5	3.4	1.1	2.2	0.7	4.7	2.3	3.7	1.7	3.9	0.8	3.9	4.4	6.8	1.0	7.4	1.8
21	Epi VM Resp (vmMYC)	7.5	14.7	2.8	2.2	12.2	4.8	12.0	2.8	2.8	0.6	14.5	4.1	8.0	4.8	8.9	1.0	5.5	2.0
22	Deep VM Resp (vmMYC)	9.5	18.6	3.5	2.8	15.5	6.0	14.9	3.4	3.0	0.7	16.9	5.0	9.7	6.0	10.6	0.8	6.2	2.1
23	Deep VM Poop (vmMYC)	5.1	10.0	1.9	1.5	8.3	3.2	8.1	1.9	1.8	0.4	9.5	2.8	5.3	3.3	5.9	0.5	3.5	1.3
24	Deep VM Mort (vmMYC)	6.0	11.7	2.2	1.8	9.8	3.8	9.5	2.2	2.1	0.5	11.1	3.2	6.3	3.8	6.9	0.6	4.1	1.5

769

770 **Table A2**. Mesozooplankton biomass and minimum respiration estimates used in the LIEM. Respiration is given in mg C m^{-2} d^{-1} and
771 biomass in mg C m^{-2}.

Quantity	P0704-1	P0704-2	P0704-4	P0810-1	P0810-2	P0810-3	P0810-4	P0810-5	P0810-6
Epipeleagic Min Resp (SAR)	8.0	8.6	8.0	0.0	0.0	0.0	0.0	8.9	0.0
SMZ Min Resp	24.4	5.1	20.6	4.8	26.3	18.0	36.3	31.6	27.3
vmSMZ Min Resp	5.3	0.4	5.5	16.4	3.3	8.6	0.0	21.5	0.0
dSMZ Min Resp	2.6	2.6	5.7	9.4	2.5	7.1	1.1	14.5	3.3
LMZ Min Resp	7.0	3.3	11.9	5.5	10.4	5.7	7.8	3.0	5.8
vmLMZ Min Resp	19.9	1.5	63.2	24.7	14.9	50.9	11.1	64.2	11.8
dLMZ Min Resp	3.2	5.4	6.7	20.4	7.6	13.3	4.9	31.3	13.5
GEL Min Resp	0.2	0.1	0.1	0.3	0.7	0.2	0.0	0.0	0.7
dGEL Min Respiration	0.4	0.1	0.5	0.4	1.1	0.3	0.1	0.4	0.8
SMZ Biomass	654	106	511	106	833	509	1249	1891	1346
vmSMZ Biomass	104	33	115	722	127	282	0	1120	0
dSMZ Biomass	499	280	715	968	307	834	111	1430	381
LMZ Biomass	424	173	478	971	586	1126	867	938	1763
vmLMZ Biomass	557	347	5175	993	1557	9859	1681	6122	1671
dLMZ Biomass	5928	2839	5702	7180	1818	3579	1395	7134	3942

2

Acknowledgements

Author contributions

ML was responsible for cruise design and protistan zooplankton data. MO was responsible for mesozooplankton data. RG was responsible for phytoplankton data. PD was responsible for myctophid data. MS was responsible for particle export data. TK and MS designed the model. TK wrote the manuscript. All authors contributed to editing the manuscript.

Conflicts of interest

The authors declare no conflicts of interest.

References

793

794 Al-Mutairi, H., and Landry, M. R. (2001). Active export of carbon and nitrogen at station ALOHA
795   by diel migrant zooplankton. *Deep-Sea Res. Part II Top. Stud. Oceanogr.* 48, 2083–2103.
796   doi:10.1016/S0967-0645(00)00174-0.

797 Anderson, T. R., Martin, A. P., Lampitt, R. S., Trueman, C. N., Henson, S. A., and Mayor, D. J.
798   (2018). Quantifying carbon fluxes from primary production to mesopelagic fish using a
799   simple food web model. *ICES J. Mar. Sci.* doi:10.1093/icesjms/fsx234.

800 Angel, M. V, and Pugh, P. R. (2010). Quantification of diel vertical migration by micronektonic
801   taxa in the northeast Atlantic. *Hydrobiologia*, 1–5. doi:10.1023/A.

802 Archibald, K. M., Siegel, D. A., and Doney, S. C. (2019). Modeling the impact of zooplankton diel
803   vertical migration on the carbon export flux of the biological pump. *Glob. Biogeochem.*
804   *Cycles*. doi:10.1029/2018GB005983.

805 Aumont, O., Maury, O., Lefort, S., and Bopp, L. (2018). Evaluating the Potential Impacts of the
806   Diurnal Vertical Migration by Marine Organisms on Marine Biogeochemistry. *Glob.*
807   *Biogeochem. Cycles* 32, 1622–1643. doi:10.1029/2018GB005886.

808 Bandara, K., Varpe, Ø., Ji, R., and Eiane, K. (2018). A high-resolution modeling study on diel and
809   seasonal vertical migrations of high-latitude copepods. *Ecol. Model.* 368, 357–376.
810   doi:10.1016/j.ecolmodel.2017.12.010.

811 Benitez-Nelson, C. R., Buesseler, K. O., Van Der Loeff, M. R., Andrews, J., Ball, L., Crossin, G., et
812   al. (2001). Testing a new small-volume technique for determining 234Th in seawater. in
813   *Journal of Radioanalytical and Nuclear Chemistry*, 795–799.
814   doi:10.1023/A:1010621618652.

815 Bianchi, D., Stock, C., Galbraith, E. D., and Sarmiento, J. L. (2013). Diel vertical migration:
816   Ecological controls and impacts on the biological pump in a one-dimensional ocean
817   model. *Glob. Biogeochem. Cycles* 27, 478–491. doi:10.1002/gbc.20031.

818 Bishop, J. K. B., Wood, T. J., Davis, R. E., and Sherman, J. T. (2004). Robotic Observations of
819   Enhanced Carbon Biomass and Export at 55°S during SOFeX. *Science* 304, 417–420.
820   doi:10.1126/science.1087717.

821 Boyd, P. W., and Trull, T. W. (2007). Understanding the export of biogenic particles in oceanic
822   waters: Is there consensus? *Prog. Oceanogr.* 72, 276–312.
823   doi:10.1016/j.pocean.2006.10.007.

824 Buesseler, K. O., and Boyd, P. W. (2009). Shedding light on processes that control particle
825   export and flux attenuation in the twilight zone of the open ocean. *Limnol. Oceanogr.* 54,
826   1210–1232. doi:10.4319/lo.2009.54.4.1210.

827   Burd, A. B., Hansell, D. A., Steinberg, D. K., Anderson, T. R., Arístegui, J., Baltar, F., et al. (2010).
828   Assessing the apparent imbalance between geochemical and biochemical indicators of
829   meso- and bathypelagic biological activity: What the @$#! is wrong with present
830   calculations of carbon budgets? *Deep-Sea Res. Part II Top. Stud. Oceanogr.* 57, 1557–
831   1571. doi:10.1016/j.dsr2.2010.02.022.

832   Choy, C. A., Popp, B. N., Hannides, C. C. S., and Drazen, J. C. (2015). Trophic structure and food
833   resources of epipelagic and mesopelagic fishes in the north pacific subtropical Gyre
834   ecosystem inferred from nitrogen isotopic compositions. *Limnol. Oceanogr.* 60, 1156–
835   1171. doi:10.1002/lno.10085.

836   Cohen, J. H., and Forward, R. B. (2009). Zooplankton Diel Vertical Migration — A Review of
837   Proximate Control. *Ocean. Mar Biol Annu Rev* 47, 77–109. doi:10.1201/9781420094220-
838   5.

839   Conover, R. J. (1966). ASSIMILATION OF ORGANIC BY ZOOPLANKTON. *Limnol. Oceanogr.* 11,
840   338–345.

841   Dam, H. G., and Peterson, W. T. (1988). The effect of temperature on the gut clearance rate
842   constant of planktonic copepods. *J. Exp. Mar. Biol. Ecol.* 123, 1–14. doi:10.1016/0022-
843   0981(88)90105-0.

844   Dam, H. G., Roman, M. R., and Youngbluth, M. J. (1995). Downward export of respiratory
845   carbon and dissolved inorganic nitrogen by diel-migrant mesozooplankton at the JGOFS
846   Bermuda time-series station. *Deep-Sea Res. Part I* 42, 1187–1197. doi:10.1016/0967-
847   0637(95)00048-B.

848   Davison, P. C., Checkley, D. M., Koslow, J. A., and Barlow, J. (2013). Carbon export mediated by
849   mesopelagic fishes in the northeast Pacific Ocean. *Prog. Oceanogr.* 116, 14–30.
850   doi:10.1016/j.pocean.2013.05.013.

851   Davison, P., Lara-Lopez, A., and Anthony Koslow, J. (2015). Mesopelagic fish biomass in the
852   southern California current ecosystem. *Deep-Sea Res. Part II Top. Stud. Oceanogr.* 112,
853   129–142. doi:10.1016/j.dsr2.2014.10.007.

854   del Giorgio, P. A., and Cole, J. J. (1998). BACTERIAL GROWTH EFFICIENCY IN NATURAL AQUATIC
855   SYSTEMS. *Annu. Rev. Ecol. Syst.* 29, 503–541. doi:10.1146/annurev.ecolsys.29.1.503.

856   del Giorgio, P. A., and Duarte, C. M. (2002). Respiration in the open ocean. *Nature* 420, 379–384.
857   doi:10.1038/nature01165.

858   Dubois, S., Del Amo, Y., Grami, B., Jude, F., Marquis, E., David, V., et al. (2012). Network analysis
859   of the planktonic food web during the spring bloom in a semi enclosed lagoon (Arcachon,
860   SW France). *Acta Oecologica* 40, 40–50. doi:10.1016/j.actao.2012.02.002.

861   Ducklow, H. W., and Harris, R. P. (1993). Introduction to the JGOFS North Atlantic bloom

862   experiment. *Deep-Sea Res. Part II* 40, 1–8. doi:10.1016/0967-0645(93)90003-6.

863 Franks, P. J. S. (2002). NPZ models of plankton dynamics: Their Construction, coupling to physics,
864   and application. *J. Oceanogr.* 58, 379–387. doi:10.1023/A:1015874028196.

865 Gasol, J. M., Alonso-Sáez, L., Vaqué, D., Baltar, F., Calleja, M. L., Duarte, C. M., et al. (2009).
866   Mesopelagic prokaryotic bulk and single-cell heterotrophic activity and community
867   composition in the NW Africa-Canary Islands coastal-transition zone. *Prog. Oceanogr.* 83,
868   189–196. doi:10.1016/j.pocean.2009.07.014.

869 Giering, S. L. C., Sanders, R., Lampitt, R. S., Anderson, T. R., Tamburini, C., Boutrif, M., et al.
870   (2014). Reconciliation of the carbon budget in the ocean's twilight zone. *Nature* 507,
871   480–483. doi:10.1038/nature13123.

872 Gontikaki, E., van Oevelen, D., Soetaert, K., and Witte, U. (2011). Food web flows through a sub-
873   arctic deep-sea benthic community. *Prog. Oceanogr.* 91, 245–259.
874   doi:10.1016/j.pocean.2010.12.014.

875 Gorsky, G., Ohman, M. D., Picheral, M., Gasparini, S., Stemmann, L., Romagnan, J.-B., et al.
876   (2010). Digital zooplankton image analysis using the ZooScan integrated system. *J.*
877   *Plankton Res.* 32, 285–303. doi:10.1093/plankt/fbp124.

878 Hannides, C. C. S., Drazen, J. C., and Popp, B. N. (2015). Mesopelagic zooplankton metabolic
879   demand in the North Pacific Subtropical Gyre. *Limnol. Oceanogr.* 60, 419–428.
880   doi:10.1002/lno.10032.

881 Hansen, A. N., and Visser, A. W. (2016). Carbon export by vertically migrating zooplankton: an
882   optimal behavior model. *Limnol. Oceanogr.* 61, 701–710. doi:10.1002/lno.10249.

883 Heitmann, C., Felmerer, G., Durmus, C., Matejic, B., and Ingianni, G. (2001). Metabolic rates of
884   epipelagic marine copepods as a function of body mass and temperature. *Mar. Biol.* 139,
885   587–596. doi:10.1007/s002270100608.

886 Henson, S. A., Sanders, R., Madsen, E., Morris, P. J., Le Moigne, F., and Quartly, G. D. (2011). A
887   reduced estimate of the strength of the ocean's biological carbon pump. *Geophys. Res.*
888   *Lett.* 38, 10–14. doi:10.1029/2011GL046735.

889 Henson, S. A., Yool, A., and Sanders, R. (2015). Variability in efficiency of particulate organic
890   carbon export: A model study. *Glob. Biogeochem. Cycles* 29, 33–45.
891   doi:10.1002/2014GB004965.

892 Hernandez-Leon, S., Olivar, M. P., Puelles, M. L., Bode, A., Castellon, A., Lopez-Perez, C., et al.
893   Zooplankton and micronekton active flux across the tropical and subtropical Atlantic
894   Ocean.

895 Ikeda, T. (1985). Metabolic rates of epipeagic marine zooplankton as a function of body mass

896   and temperature. *Mar. Biol.* 85, 1–11.

897   Ikeda, T., Kanno, Y., Ozaki, K., and Shinada, A. (2001). Metabolic rates of epipelagic marine
898   copepods as a function of body mass and temperature. *Mar. Biol.* 139, 587–596.
899   doi:10.1007/s002270100608.

900   Jackson, G. A., and Eldridge, P. M. (1992). Food web analysis of a planktonic system off
901   Southern California. *Prog. Oceanogr.* 30, 223–251. doi:10.1016/0079-6611(92)90014-Q.

902   Kiko, R., Hauss, H., Christiansen, S., Faustmann, J., and Rodrigues, E. Zooplankton-mediated
903   fluxes in the Eastern Tropical North Pacific. *Front. Mar. Sci.*

904   Knauer, G. A., Martin, J. H., and Bruland, K. W. (1979). Fluxes of particulate carbon, nitrogen,
905   and phosphorus in the upper water column of the northeast Pacific. *Deep Sea Res. Part
906   Oceanogr. Res. Pap.* 26, 97–108. doi:10.1016/0198-0149(79)90089-X.

907   Kones, J. K., Soetaert, K., van Oevelen, D., and Owino, J. O. (2009). Are network indices robust
908   indicators of food web functioning? A Monte Carlo approach. *Ecol. Model.* 220, 370–382.
909   doi:10.1016/j.ecolmodel.2008.10.012.

910   Krause, J. W., Brzezinski, M. A., Goericke, R., Landry, M. R., Ohman, M. D., Stukel, M. R., et al.
911   (2015). Variability in diatom contributions to biomass, organic matter production and
912   export across a frontal gradient in the California Current Ecosystem. *J. Geophys. Res.
913   Oceans* 120, 1032–1047. doi:10.1002/2014JC010472.

914   Kroes, H. W. (1977). The niche structure of ecosystems. *J. Theor. Biol.* 65, 317–326.
915   doi:10.1016/0022-5193(77)90327-7.

916   Landry, M. R., Brown, S. L., Rii, Y. M., Selph, K. E., Bidigare, R. R., Yang, E. J., et al. (2008). Depth-
917   stratified phytoplankton dynamics in Cyclone Opal, a subtropical mesoscale eddy. *Deep
918   Sea Res. Part II Top. Stud. Oceanogr.* 55, 1348–1359. doi:10.1016/j.dsr2.2008.02.001.

919   Landry, M. R., Ohman, M. D., Goericke, R., Stukel, M. R., Barbeau, K. A., Bundy, R., et al. (2012).
920   Pelagic community responses to a deep-water front in the California Current Ecosystem:
921   Overview of the A-Front Study. *J. Plankton Res.* 34, 739–748. doi:10.1093/plankt/fbs025.

922   Landry, M. R., Ohman, M. D., Goericke, R., Stukel, M. R., and Tsyrklevich, K. (2009). Lagrangian
923   studies of phytoplankton growth and grazing relationships in a coastal upwelling
924   ecosystem off Southern California. *Prog. Oceanogr.* 83, 208–216.
925   doi:10.1016/j.pocean.2009.07.026.

926   Laws, E. A., D'Sa, E., and Naik, P. (2011). Simple equations to estimate ratios of new or export
927   production to total production from satellite-derived estimates of sea surface
928   temperature and primary production. *Limnol. Oceanogr. Methods* 9, 593–601.
929   doi:10.4319/lom.2011.9.593.

930   Longhurst, A. R., Bedo, A. W., Harrison, W. G., Head, E. J. H., and Sameoto, D. D. (1990). Vertical
931   flux of respiratory carbon by oceanic diel migrant biota. *Deep Sea Res. Part Oceanogr.*
932   *Res. Pap.* 37, 685–694. doi:10.1016/0198-0149(90)90098-G.

933   Marra, J. (2009). Net and gross productivity: Weighing in with 14C. *Aquat. Microb. Ecol.* 56,
934   123–131. doi:10.3354/ame01306.

935   Milligan, A. J., Halsey, K. H., and Behrenfeld, M. J. (2014). HORIZONS:Advancing interpretations
936   of 14C-uptake measurements in the context of phytoplankton physiology and ecology. *J.*
937   *Plankton Res.* 37, 692–698. doi:10.1093/plankt/fbv051.

938   Minas, H. J., Le B. Williams, P. J., Robinson, C., Woodward, E. M. S., Lefevre, D., and Minas, M.
939   (2002). Review of gross community production, primary production, net community
940   production and dark community respiration in the Gulf of Lions. *Deep Sea Res. Part II*
941   *Top. Stud. Oceanogr.* 44, 801–832. doi:10.1016/s0967-0645(96)00091-4.

942   Morales, C. E. (1999). Carbon and nitrogen fluxes in the oceans: the contribution by
943   zooplankton migrants to active transport in the North Atlantic during the Joint Global
944   Ocean Flux Study. *J. Plankton Res.* 21, 1799–1808. doi:10.1093/plankt/21.9.1799.

945   Morozov, A. Y., and Kuzenkov, O. A. (2016). Towards developing a general framework for
946   modelling vertical migration in zooplankton. *J. Theor. Biol.* 405, 17–28.
947   doi:10.1016/j.jtbi.2016.01.011.

948   Morrow, R. M., Ohman, M. D., Goericke, R., Kelly, T. B., Stephens, B. M., and Stukel, M. R.
949   (2018). CCE V: Primary production, mesozooplankton grazing, and the biological pump
950   in the California Current Ecosystem: Variability and response to El Niño. *Deep-Sea Res.*
951   *Part Oceanogr. Res. Pap.* 140, 52–62. doi:10.1016/j.dsr.2018.07.012.

952   Ohman, M. D., Powell, J. R., Picheral, M., and Jensen, D. W. (2012). Mesozooplankton and
953   particulate matter responses to a deep-water frontal system in the southern California
954   Current System. *J. Plankton Res.* 34, 815–827. doi:10.1093/plankt/fbs028.

955   Ohman, M. D., and Romagnan, J. B. (2016). Nonlinear effects of body size and optical
956   attenuation on Diel Vertical Migration by zooplankton. *Limnol. Oceanogr.* 61, 765–770.
957   doi:10.1002/lno.10251.

958   Omand, M. M., Lee, C. M., Perry, M. J., Briggs, N., Cetini, I., Mahadevan, A., et al. (2015). Eddy-
959   driven subduction exports particulate organic carbon from the spring bloom. *Science*
960   348, 222–225. doi:10.1126/science.1260062.

961   Peterson, B. J. (1980). PRODUCTIVITY AND THE 14C-CO2 METHOD : A History of the
962   Productivity Problem. *Ecology* 11, 359–385.

963   Pike, S. M., Buesseler, K. O., Andrews, J., and Savoy, N. (2005). Quantification of234Th
964   recovery in small volume sea water samples by inductively coupled plasma-mass

965   spectrometry. *J. Radioanal. Nucl. Chem.* 263, 355–360. doi:10.1007/s10967-005-0062-9.

966   Powell, J. R., and Ohman, M. D. (2012). Use of glider-class acoustic Doppler profilers for
967   estimating zooplankton biomass. *J. Plankton Res.* 34, 563–568.
968   doi:10.1093/plankt/fbs023.

969   Powell, J. R., and Ohman, M. D. (2015). Changes in zooplankton habitat, behavior, and acoustic
970   scattering characteristics across glider-resolved fronts in the Southern California Current
971   System. *Prog. Oceanogr.* 134, 77–92. doi:10.1016/j.pocean.2014.12.011.

972   Robinson, C., Steinberg, D. K., Anderson, T. R., Arístegui, J., Carlson, C. A., Frost, J. R., et al.
973   (2010). Mesopelagic zone ecology and biogeochemistry – a synthesis. *Deep Sea Res. Part*
974   *II Top. Stud. Oceanogr.* 57, 1504–1518. doi:10.1016/j.dsr2.2010.02.018.

975   Sailley, S. F., Ducklow, H. W., Moeller, H. V, Fraser, W. R., Schofield, O. M., Steinberg, D. K., et al.
976   (2013). Carbon fluxes and pelagic ecosystem dynamics near two western Antarctic
977   Peninsula Adélie penguin colonies: An inverse model approach. *Mar. Ecol. Prog. Ser.* 492,
978   253–272. doi:10.3354/meps10534.

979   Saint-béat, B., Vézina, A. F., Asmus, R., Asmus, H., and Niquil, N. (2013). The mean function
980   provides robustness to linear inverse modelling flow estimation in food webs : A
981   comparison of functions derived from statistics and ecological theories. *Ecol. Model.* 258,
982   53–64. doi:10.1016/j.ecolmodel.2013.01.023.

983   Samo, T. J., Pedler, B. E., Ball, G. I., Pasulka, A. L., Taylor, A. G., Aluwihare, L. I., et al. (2012).
984   Microbial distribution and activity across a water mass frontal zone in the California
985   Current Ecosystem. *J. Plankton Res.* 34, 802–814. doi:10.1093/plankt/fbs048.

986   Savoye, N., Benitez-Nelson, C., Burd, A. B., Cochran, J. K., Charette, M., Buesseler, K. O., et al.
987   (2006). 234Th sorption and export models in the water column: A review. *Mar. Chem.*
988   100, 234–249. doi:10.1016/j.marchem.2005.10.014.

989   Siegel, D. A., Buesseler, K. O., Doney, S. C., Sailley, S. F., Behrenfeld, M. J., and Boyd, P. W.
990   (2014). Global assessment of ocean carbon export by combining satellite observations
991   and food-web models. *Glob. Biogeochem. Cycles* 28, 181–196.
992   doi:10.1002/2013GB004743.

993   Steinberg, D. K., Carlson, C. A., Bates, N. R., Goldthwait, S. A., Madin, L. P., and Michaels, A. F.
994   (2000). Zooplankton vertical migration and the active transport of dissolved organic and
995   inorganic carbon in the Sargasso Sea. *Deep Sea Res. Part Oceanogr. Res. Pap.* 47, 137–
996   158. doi:10.1016/S0967-0637(99)00052-7.

997   Steinberg, D. K., and Landry, M. R. (2017). Zooplankton and the Ocean Carbon Cycle. *Annu. Rev.*
998   *Mar. Sci.* 9, 413–444. doi:10.1146/annurev-marine-010814-015924.

999   Steinberg, D. K., Van Mooy, B. A. S., Buesseler, K. O., Boyd, P. W., Kobari, T., and Karl, D. M.

1000   (2008). Bacterial vs. zooplankton control of sinking particle flux in the ocean's twilight
1001   zone. *Limnol. Oceanogr.* 53, 1327–1338. doi:10.4319/lo.2008.53.4.1327.

1002   Straile, D. (1997). Gross Growth Efficiencies of Protozoan and Metazoan Zooplankton and Their
1003   Dependence on Food Concentration , Predator-Prey Weight Ratio, and Taxonomic
1004   Group. *Limnol. Oceanogr.* 42, 1375–1385.

1005   Stukel, M. R., Décima, M., and Kelly, T. B. (2018a). A new approach for incorporating 15N
1006   isotopic data into linear inverse ecosystem models with Markov Chain Monte Carlo
1007   sampling. *PLoS ONE* 13. doi:10.1371/journal.pone.0199123.

1008   Stukel, M. R., Décima, M., Landry, M. R., and Selph, K. E. (2018b). Nitrogen and Isotope Flows
1009   Through the Costa Rica Dome Upwelling Ecosystem: The Crucial Mesozooplankton Role
1010   in Export Flux. *Glob. Biogeochem. Cycles* 32, 1815–1832. doi:10.1029/2018GB005968.

1011   Stukel, M. R., Kahru, M., Benitez-Nelson, C. R., Décima, M., Goericke, R., Landry, M. R., et al.
1012   (2015). Using Lagrangian-based process studies to test satellite algorithms of vertical
1013   carbon flux in the eastern North Pacific Ocean. *J. Geophys. Res. Oceans* 120, 7208–7222.
1014   doi:10.1002/2015JC011264.

1015   Stukel, M. R., Kelly, T. B., Aluwihare, L. I., Barbeau, K. A., Goericke, R., Krause, J. W., et al. (2019).
1016   The Carbon:234Thorium ratios of sinking particles in the California current ecosystem 1:
1017   relationships with plankton ecosystem dynamics. *Mar. Chem.*, #pagerange#.
1018   doi:10.1016/j.marchem.2019.01.003.

1019   Stukel, M. R., Landry, M. R., Ohman, M. D., Goericke, R., Samo, T., and Benitez-nelson, C. R.
1020   (2012). Do inverse ecosystem models accurately reconstruct plankton trophic fl ows￼?
1021   Comparing two solution methods using fi eld data from the California Current. *J. Mar.*
1022   *Syst.* 91, 20–33. doi:10.1016/j.jmarsys.2011.09.004.

1023   Stukel, M. R., Ohman, M. D., Kelly, T. B., and Biard, T. The roles of filter-feeding and flux-feeding
1024   zooplankton as gatekeepers of particle flux into the mesopelagic ocean. *Front. Mar. Sci.*

1025   Stukel, M. R., Ohman, M. M. D., Benitez-Nelson, C. R. C., and Landry, M. M. R. (2013).
1026   Contributions of mesozooplankton to vertical carbon export in a coastal upwelling
1027   system. *Mar. Ecol. Prog. Ser.* 491, 47–65. doi:10.3354/meps10453.

1028   Stukel, M. R., Song, H., Goericke, R., and Miller, A. J. (2018c). The role of subduction and
1029   gravitational sinking in particle export, carbon sequestration, and the remineralization
1030   length scale in the California Current Ecosystem. *Limnol. Oceanogr.* 63, 363–383.
1031   doi:10.1002/lno.10636.

1032   Tanaka, T., and Rassoulzadegan, F. (2004). Vertical and seasonal variations of bacterial
1033   abundance and production in the mesopelagic layer of the NW Mediterranean Sea:
1034   Bottom-up and top-down controls. *Deep-Sea Res. Part Oceanogr. Res. Pap.* 51, 531–544.
1035   doi:10.1016/j.dsr.2003.12.001.

1036   Taylor, A. G., Goericke, R., Landry, M. R., Selph, K. E., Wick, D. A., and Roadman, M. J. (2012).
1037   Sharp gradients in phytoplankton community structure across a frontal zone in the
1038   California Current Ecosystem. *J. Plankton Res.* 34, 778–789. doi:10.1093/plankt/fbs036.

1039   van den Meersche, K., Soetaert, K., van Oevelen, D., Meersche, K. Van den, Soetaert, K., and
1040   Oevelen, D. Van (2009). xsample(): An R Function for Sampling Linear Inverse Problems.
1041   Journal of Statistical Software. *J. Stat. Softw. Code Snippets* 30, 1–15.
1042   doi:10.1002/wics.10.

1043   van Oevelen, D., Soetaert, K., and Heip, C. (2012). Carbon flows in the benthic food web of the
1044   Porcupine Abyssal Plain: The (un)importance of labile detritus in supporting microbial
1045   and faunal carbon demands. *Limnol. Oceanogr.* 57, 645–664.
1046   doi:10.4319/lo.2012.57.2.0645.

1047   van Oevelen, D., van den Meersche, K., Meysman, F. J. R., Soetaert, K., Middelburg, J. J., and
1048   Vézina, A. F. (2010). Quantifying food web flows using linear inverse models. *Ecosystems*
1049   13, 32–45. doi:10.1007/s10021-009-9297-6.

1050   Vézina, A., Platt, T., Vezina, A. F., and Platt, T. (1988). Food web dynamics in the ocean. I. Best-
1051   estimates of flow networks using inverse methods. *Mar. Ecol. Prog. Ser.* 42, 269–287.
1052   doi:10.3354/meps042269.

1053   Wilson, S. E., Steinberg, D. K., and Buesseler, K. O. (2008). Changes in fecal pellet characteristics
1054   with depth as indicators of zooplankton repackaging of particles in the mesopelagic
1055   zone of the subtropical and subarctic North Pacific Ocean. *Deep Sea Res. Part II Top.*
1056   *Stud. Oceanogr.* 55, 1636–1647. doi:10.1016/j.dsr2.2008.04.019.

1057   Wilson, S. E., Steinberg, D. K., Chu, F.-L. E., and Bishop, J. K. B. (2010). Feeding ecology of
1058   mesopelagic zooplankton of the subtropical and subarctic North Pacific Ocean
1059   determined with fatty acid biomarkers. *Deep Sea Res. Part Oceanogr. Res. Pap.* 57,
1060   1278–1294. doi:10.1016/j.dsr.2010.07.005.

1061   Yebra, L., Almeida, C., and Hernández-León, S. (2005). Vertical distribution of zooplankton and
1062   active flux across an anticyclonic eddy in the Canary Island waters. *Deep-Sea Res. Part*
1063   *Oceanogr. Res. Pap.* 52, 69–83. doi:10.1016/j.dsr.2004.08.010.

1064   Yokokawa, T., Yang, Y., Motegi, C., and Nagata, T. (2013). Large-scale geographical variation in
1065   prokaryotic abundance and production in meso- and bathypelagic zones of the central
1066   Pacific and Southern ocean. *Limnol. Oceanogr.* 58, 61–73.
1067   doi:10.4319/lo.2013.58.1.0061.

1068

1069